MICROSTRUCTURAL AND METAMORPHIC ANALYSIS OF THE MALTON GNEISS DOME, SOUTHERN CANADIAN CORDILLERA

A Thesis

Presented to

the Faculty of the Department of Earth and Atmospheric Sciences

University of Houston

In Partial Fulfillment

of the Requirements for the Degree

Master of Science

By

Hana Kabazi

August 2013

Microstructural and Metamorphic Analysis of the Malton Gneiss Dome, southern Canadian Cordillera

_____

Hana Kabazi

APPROVED:

_____

Dr. Alexander Robinson, Advisor

_____

Dr. Virginia Sisson, Committee Member

_____

Dr. Michael Murphy, Committee Member

_____

Dr. Jerome Guynn, Committee Member

_____

Dean, College of Natural Science and Mathematics

Acknowledgements

I would like to thank Dr. Alexander Robinson for accepting me as his graduate student, and his continuous guidance and help with my project. I thank Virginia Sisson for all of her support, and input, as well as my other committee members, Michael Murphy and Jerome Guynn. I would like to thank Wendy Nelson for all of her wisdom, especially with the electron microprobe. Finally, I'd especially like to thank my mom and dad, as well as all of my friends, for their continuous support and encouragement throughout the years.

MICROSTRUCTURAL AND METAMORPHIC ANALYSIS OF THE MALTON GNEISS DOME, SOUTHERN CANADIAN CORDILLERA

An Abstract of a Thesis

Presented to

the Faculty of the Department of Earth and Atmospheric Sciences

University of Houston

In Partial Fulfillment

of the Requirements for the Degree

Master of Science

By

Hana Kabazi

August 2013

Abstract

The Malton Gneiss Dome is located in the Southern Canadian Cordillera, at the northern most tip of the Shuswap Metamorphic Core Complex (SMCC). It is one of four domes within the SMCC, and is located closest to the foreland. Although deformation fabrics within the SMCC are dominated by E-W/NE-SW verging deformation fabrics, deformation fabrics within the Malton Gneiss Dome show top-NW sense of shear, parallel to the orogenic front. One possible explanation for this difference is the tectonically forced orogen parallel flow model, where foreland directed flow of low-viscosity mid-lower crust encounters a barrier, either thermal or structural, forcing it to flow laterally/parallel to the orogen. This model predicts that orogen parallel fabrics are synchronous with peak metamorphic conditions, during the late-Cretaceous to early-Cenozoic. Peak metamorphic conditions were investigated though quantitative thermobarometry and the relationship between deformation and metamorphism assessed through quartz deformation fabrics. My results show all samples analyzed have experienced amphibolite facies pressure and temperature conditions, with ranges of 600- 775 ^{0}C and 400-900 MPa. These conditions are similar to the other domes within the complex. Petrofabric analysis confirmed the orogen parallel movement within the dome coincided with peak metamorphic conditions, indicated by both syn-kinematic garnet and feldspar porphyroblasts which record peak metamorphic conditions.

Table of Contents

1. Introduction.....1

2. Geologic Setting.....1

3. Models of Ductile Deformation within Continental Orogens.....9

4. Structural Formation of Domes in the Shuswap Metamorphic Core Complex.....11

5. Structural Observations from the Malton Dome 14

6. Tectonically Forced Orogen Parallel Flow.....15

7. Methods 16

7.1 Electron Microprobe 16

7.2 Garnet Analysis 17

7.3 Feldspar Analysis 19

7.4 Amphibole & Mica Analysis 21

7.5 Geothermometry and Geobarometry.....21

8. Results.....22

8.1 P-T Conditions.....22

8.2 Petrofabric Observations.....33

9. Discussion 35

9.1 P-T Data.....35

9.2 Petrofabric Observations.....38

9.3 Regional Implications.....39

10. Conclusions.....41

1. Introduction

The Malton Gneiss Dome, which consists of Archean metasediments and metaigneous rocks, is located at the northern tip of the Shuswap Metamorphic Core Complex (SMCC) in the southern Canadian Cordillera (Fig 1) (Morrison 1982). The Malton dome is the northernmost gneiss dome in the SMCC, and has a distinct deformation fabric from the others (Morrison 1982). Unlike the gneiss domes exposed to the south, which display predominately E-W trending orogen perpendicular deformation, fabrics within the core of the Malton Dome indicate top to the NW-directed orogen parallel flow (McDonough and Simony 1988, McDonough and Simony 1989). My research focused on determining peak metamorphic conditions from four samples located with the dome, integrated with petrofabric observations to attempt to connect orogen parallel deformation with peak metamorphism within the area.

2. Geologic Setting

The tectonic evolution of the Canadian Cordillera was characterized by a long lived convergent margin during the Mesozoic, which involved the accretion of several arc terrains onto the western coast of the North American Craton (Gordon et al. 2008). Deformation throughout the region consisted of folding, thrusting, intrusion of batholiths, and crustal thickening in the Jurassic and Cretaceous (Fig 2), followed by Paleocene to Eocene extension and orogenic collapse (Gordon et al. 2008).

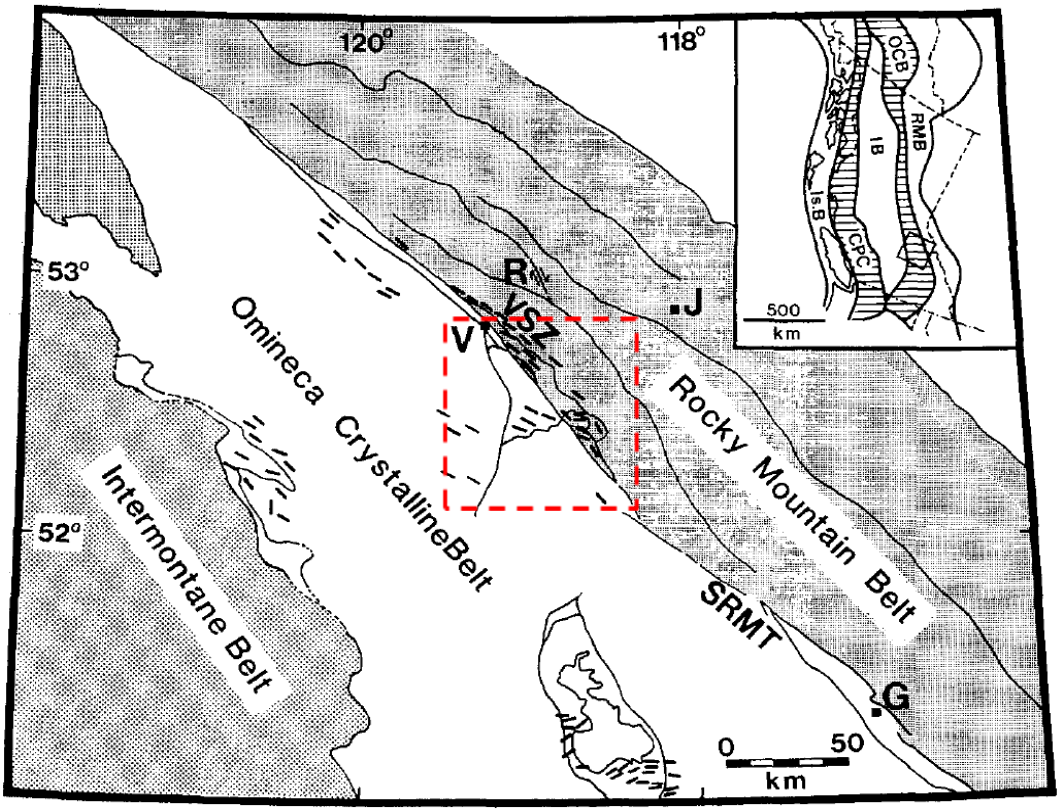

Fig 1: General map of the Omineca Crystalline Belt; R=Resplendent fault, VSV=Valemount strain zone, V=Valemount, J=Jasper, SRMT= Southern Rocky Mountain Trench, G= Golden. Red dashed line indicates location of the Malton dome (McDonough and Simony 1989)

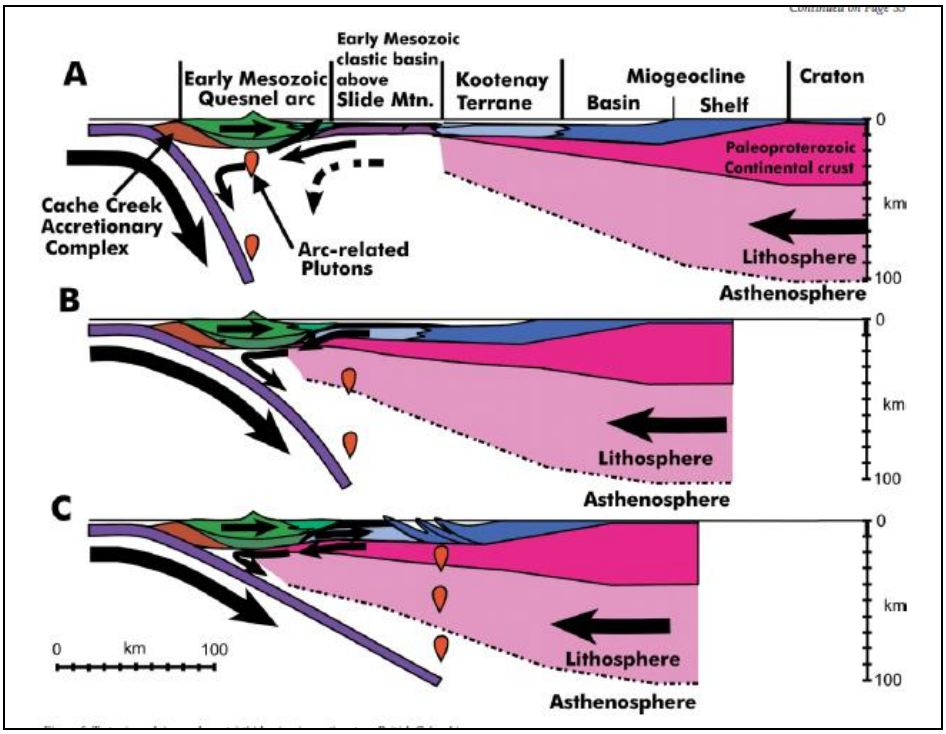

Fig 2: Simplified tectonic evolution of the Southern Canadian Cordillera, showing continuous convergence throughout the Jurassic. a) early Jurassic, b) late-early Jurassic, c) early-mid Jurassic (Monger and Price 2002)

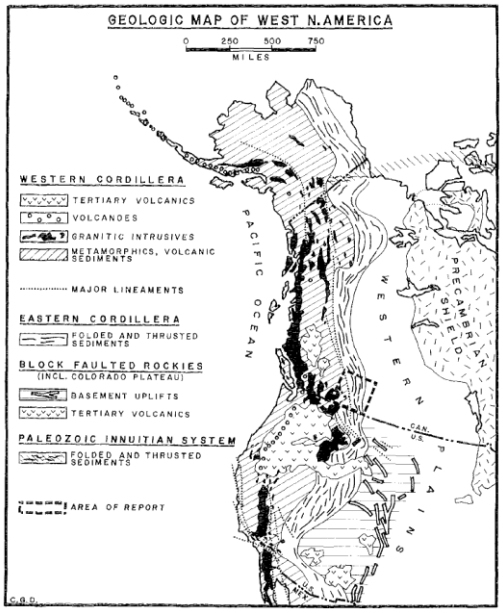

Fig 3: Regional map of the western portion of North America (Bally et al. 1966). Box shows the study area of Bally.

The southern Canadian Cordillera is about 900km wide (Fig 3), and can be separated in to five different tectonic terrains; the Insular, Coast, Intermontane, Omineca, and Foreland belts (Fig 4) (Gervais et al. 2010). In the early Jurassic (~185 Ma) convergence of the western continental Paleozoic passive margin with offshore subduction zones occurred, followed by the accretion of arc material onto the western continental Paleozoic passive margin (Monger & Price 2002). By 90 Ma, in the Late Cretaceous, a new continental active margin developed (Monger & Price 2002). The deformation and metamorphism of the Cordillera occurred predominately in the Jurassic and Cretaceous, mostly in the Coast and Omineca belt areas (Brown et al. 1986, Gervais et al. 2010).

The Omineca belt (Fig 1) is located within the hinterland of the Rocky Mountain Belt. It is the easternmost exposure of upper amphibolite to granulite facies rocks (Gordon et al. 2008), and is composed of sedimentary, volcanic, and granitic rocks (Monger & Price 2002, Norlander et al. 2002). The Omineca belt is thought to override a group of deformed basement slices separated by ductile shear zones, to account for at least another 100 km of the shortening that is not accounted for in the foreland by the eastward thrusting and movement of the Monashee Decollement (Brown et al. 1986).

The Shuswap Metamorphic core complex (SMCC) is the largest of the core complexes within the Canadian Cordillera (Norlander et al. 2002). It is located within the hinterland of the Rocky Mountain fold and thrust belt, in the southern

portion of the Omineca belt and was exhumed during the Eocene to Oligocene (Norlander et al. 2002). The SMCC is composed of variously metamorphosed lithologies including: Early Proterozoic crystalline basement; mid-Proterozoic

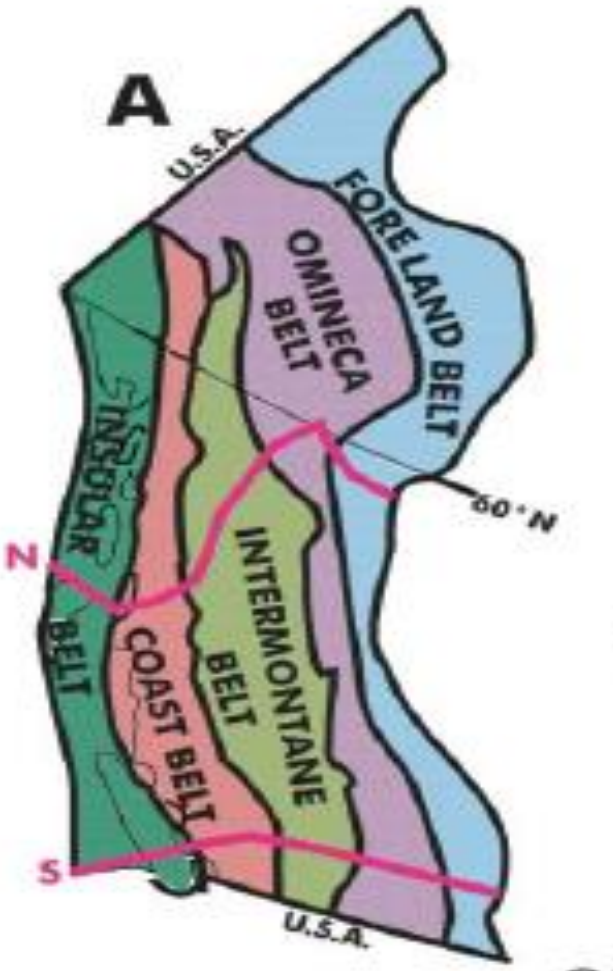

Fig 4: Canadian Cordillera broken into 5 different mountain belts (Monger and Price 2002)

sediments, which filled a rift basin; late Proterozoic to Paleozoic-Triassic sediments deposited along a passive margin; and lastly allochthonous oceanic rocks, including Paleozoic to Triassic volcanic arcs and granitic batholiths (Armstrong 1982). It represents the exposed metamorphic core of the southern Canadian Cordillera, and is part of the Omineca belt located in the southeastern part of British Columbia (Coney and Harms 1984, Gordon et al. 2008). The SMCC is bound to the east by the Eocene top-east high angle Southern Rocky Mountain Trench normal fault and the Purcell Thrust, and bound to the west by part of the Eocene low angled Okanagan-Eagle River fault system, locally called the Thompson fault (Fig 5) (Sevigney et al. 1990, McDonough & Simony 1988). During the Cretaceous major crustal thickening occurred, resulting in production of the 4 main domes within the complex; Valhalla, Thor-Odin, Frenchman Cap, and the Malton, from south to north (Armstrong 1982, Norlander et al. 2002) (Fig 6). Peak metamorphism of the SMCC occurred between the late-Cretaceous to early-Cenozoic. (Morrison1982, Norlander et al. 2002).Deformation within the area ended in the Middle Eocene at about 45 Ma after a period of crustal heating and extension (Armstrong 1982, Gordon et al. 2008). The Shuswap Metamorphic Core Complex is bound by both low angle detachment zones, and high angle normal faults, which accommodated exhumation of the high grade metamorphic rocks (Norlander et al. 2002). The rocks within the Shuswap Metamorphic Core Complex are highly metamorphosed, with extensive ductile deformation, predominately trending E-W to NE-SW (Fig 7) (Cowgill 1994). This

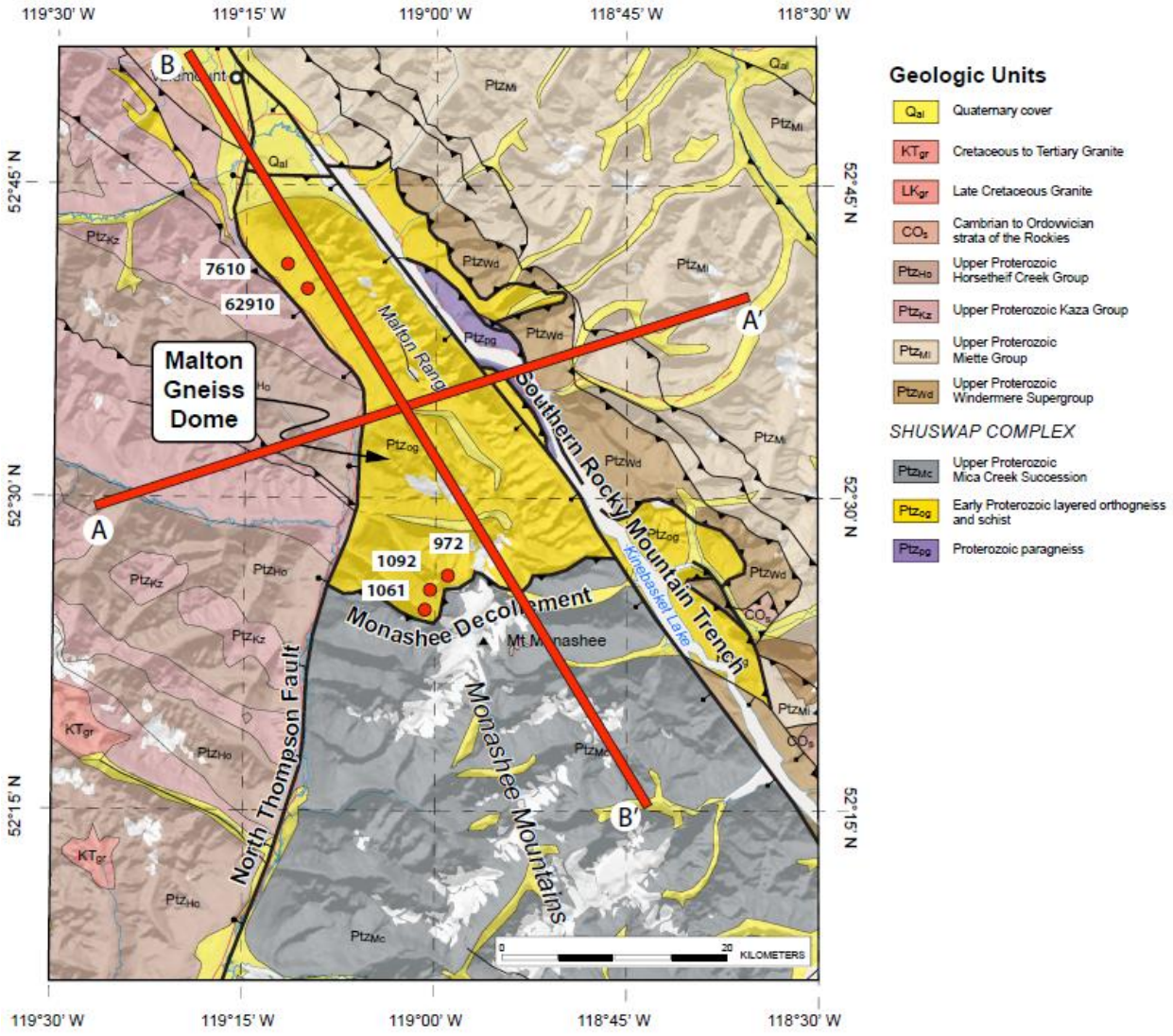

Fig 5: A general map of the Malton Dome within the SMCC. The red lines indicate 2 cross-sections, Fig. 19. The red points show the location of the samples that were analyzed in this study.

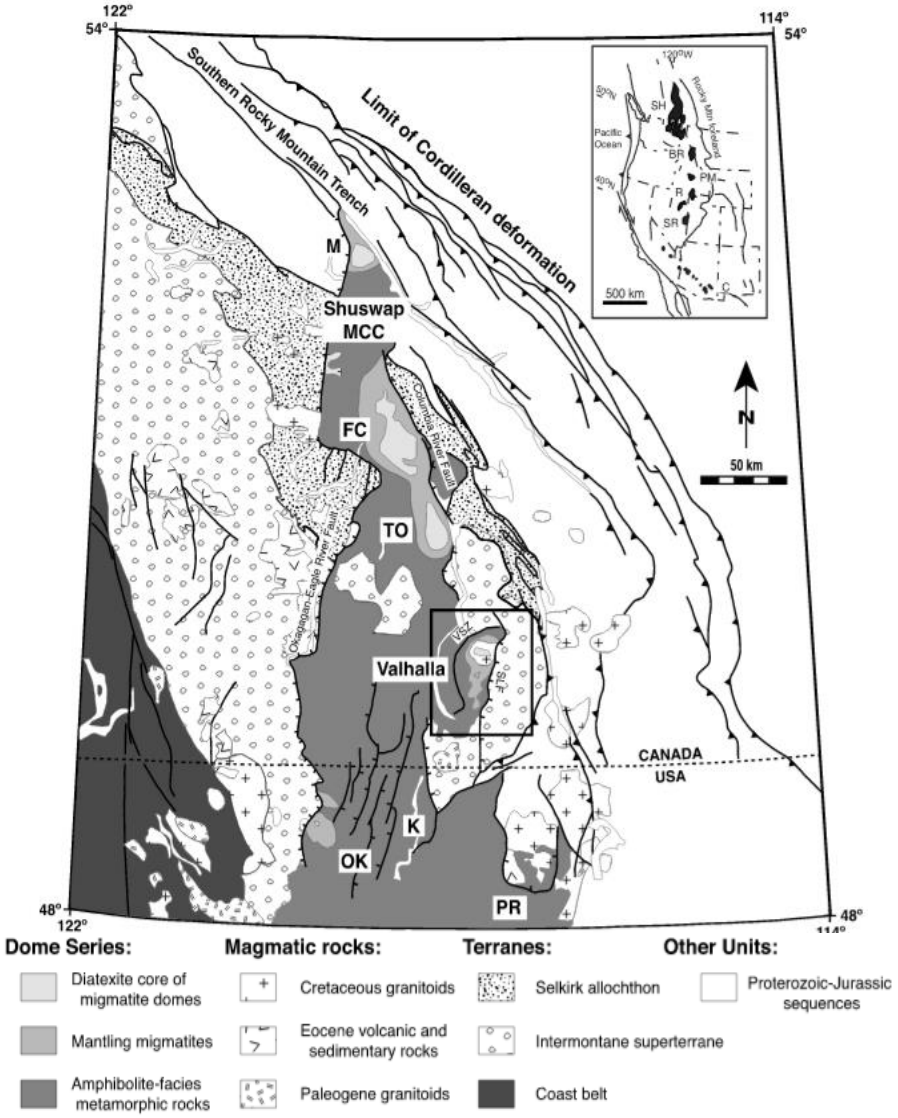

Fig 6: Location of the Shuswap Metamorphic Core Complex (SMCC), as well as the domes within it; M= Malton, FC= Frenchman Ca, TO= Thor-Odin, V= Valhalla, which was Gordon's study area (Gordon et al. 2008)

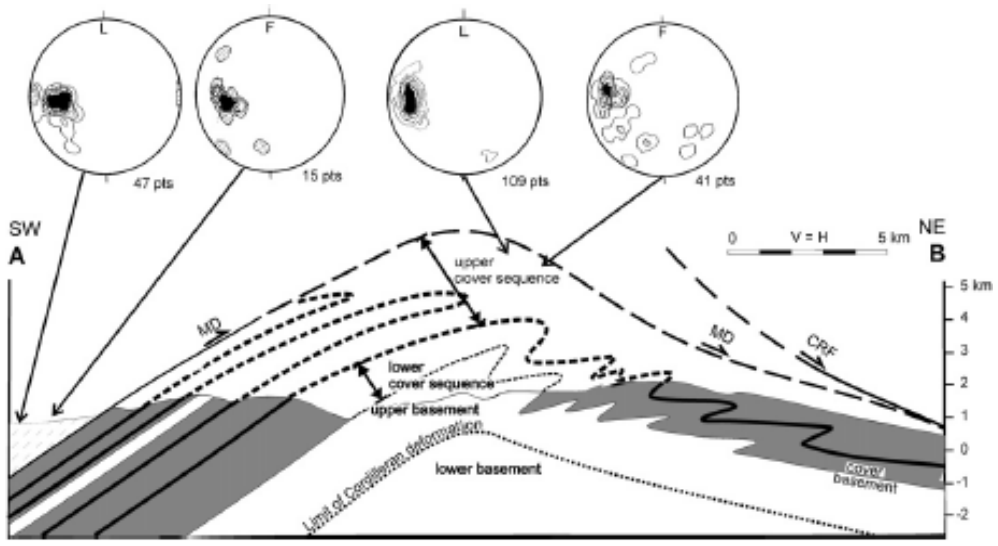

Fig 7: Lineations from the Frenchman cap trending E-W, as seen in most of the SMCC; MD= Monashee Decollement, CRF= Columbia River Fault (Gervais et al. 2010)

trend is seen in all of the domes within the SMCC with the exception of the Malton dome (Cowgill 1994).

3. Models of Ductile Deformation within Continental Orogens

There are four general models that have been proposed to explain ductile deformation in the hinterland of orogenic belts including the channel flow model (Fig 8) (e.g. Beaumont et al. 2001) Hinterland crustal thickening leads to widespread crustal melting and a decrease in viscosity. This together with a large difference in gravitational potential energy, drives the low-viscosity towards the foreland as channelized flow in the middle crust. Flow is interpreted to move towards the foreland, from the hinterland, with a triangular shape at the tip to accommodate movement. This process is thought to be driven by melting of the middle and lower crust causing the decrease in viscosity needed for the flow.

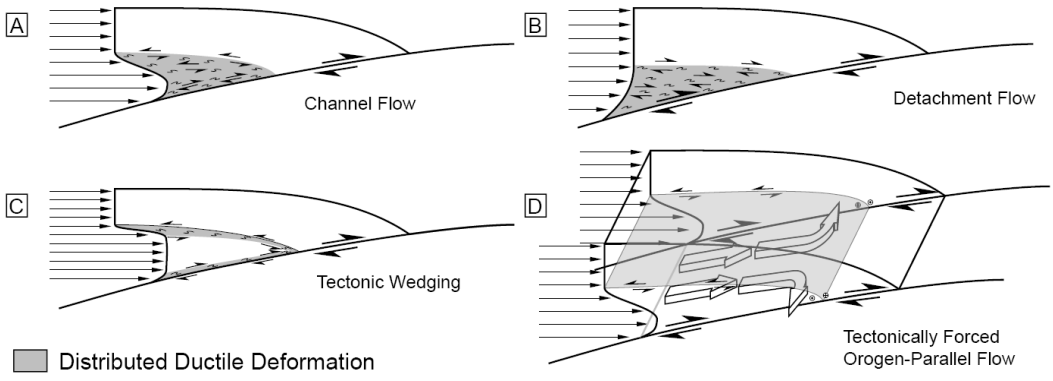

Fig 8: Four models for ductile deformation. These include: a) channel flow, b) detachment flow, c) tectonic wedging, d) tectonically forced orogen parallel flow (Robinson and Sisson 2011)

The detachment flow model (Fig 8) (Carr and Simony, 2006) is based on the consistent top-to the foreland directed shear sense of deformation fabrics found throughout the SMCC. This is interpreted to be recording the distributed simple shear during a foreland directed transport of allochthonous material.

The third model, tectonic wedging (Fig 8) (Yin 2006, Webb et al. 2007), describes the movement of a more stable middle to lower crustal sheet, bound by localized shear zones, towards the foreland. This model requires a structurally higher shear zone, acting as a passive roof thrust moving towards the hinterland (Yin 2006, Webb et al. 2007).

Finally, there is the tectonically forced orogen parallel flow model (Fig 8) (Hatcher and Merschat 2006). The initial mechanisms of movement are similar to channel flow, but this model proposes that flow may encounter a barrier, structural or thermal, while moving towards the foreland. The ductally flowing crust is forced

to flow laterally when it reaches this barrier, due to the continued foreland directed movement in the hinterland (Hatcher and Merschat 2006). Orogen parallel flow has been interpreted to have occurred in the hinterland of the Inner Piedmont of the Southern Appalachians, where observations documented orogen parallel flow in regions closest to the foreland (Hatcher and Merschat 2006) This model may provide an important framework for the structural data from the Malton dome, due to the orogen parallel lineations as well as the proximity to the foreland relative to the rest of the SMCC.

4. Structural Formation of Domes in the Shuswap Metamorphic Core Complex

There are four major domes within the SMCC which are, from south to north; the Valhalla dome, the Thor-Odin dome, the Frenchman Cap dome, and the Malton dome (Table 1) Fig 6). The three southern domes are located within the hanging wall of the Monashee Decollement. The Malton dome, located closest to the foreland and the Southern Rocky Mountain Trench (SRMT), is within the footwall of the decollement. The Valhalla dome, like the majority of the SMCC, is dominated by E-W trending lineations and has kinematic indicators which show top to the east movement (Gordon et al. 2008). This movement is associated with the Gwillim Creek shear zone. Shortening began in the Cretaceous, at ~66 Ma, causing deformation in the area (Gordon et al. 2008). There are abundant migmatites and leucogranites, and their close relationship to deformation fabrics show that partial melting was important to the tectonic evolution of the Valhalla complex during the

Paleocene (Gordon et al. 2008). Peak metamorphism has been reported to have reached temperatures of up to 850 ^{0}C and pressures of up to 730

	Valhalla	Thor-Odin	Frenchman Cap
lithology	Metapelites, and granitic bodies	3 superposed crustal units (exposed rock); M: metapelitic schist, calc silicates, marble, amphibolite, & quartzite; L: gedrite-cordierite rocks interbedded with migmatitic sillimanite and K-feldspar metapelitic rocks, garnet, hornblende, amphibole, & granitoids	Paleozoic and Proterozoic Orthogneisses
Metamorphic grade	Amphibolite-Granulite	Amphibolite-Upper Amphibolite (even into granulite)	Upper Cover: Kyanite - K-feldspar; Lower cover: Sillimanite
Start of Metamorphism	`66 Ma	62-56Ma	60-55Ma.
End of Metamorphism	51-45 Ma (Gordon et al. 2008)		
Deformation Fabrics & Sense of Shear	E-W lineations, with a top to the E. movement	Middle: Shallowly dipping E-W/NE-SW lineations; Lower: E-W mineral lineations, thought to show evidence of decompression	Upper cover: E verging penetrative ductile deformation; Lower Cover: E. verging deformation; Upper basement: penetrative Eocene deform: Lower basement: No penetrative deformation
Other notes	said to be the structurally highest out of all of the domes within the SMCC		Doming thought to be because of incipient drag folding following a thrust above a basement ramp
Sources	Gordon et al. 2008	Norlander et al. 2002	Gervais et al. 2010

Table 1: Summary of the geologic features of the other 3 domes within the SMCC

MPa (Carr and Simony 2006). This places the rocks within the Valhalla at upper amphibolite to granulite facies conditions. Deformation is thought to have stopped around 45Ma in the mid Eocene, which corresponds to the end of deformation within the entire SMCC (Coney & Harms 1984, Armstrong 1982, Gordon et al. 2008).

The Thor-Odin dome lies to the north of the Valhalla dome, like the Valhalla dome, it is dominated by E-W lineations (Norlander 2002) (Fig 6). Deformation is thought to have begun 62-56 Ma, slightly later than the Valhalla dome, and reached the upper amphibolite facies, possibly granulite facies, but peak temperatures are not thought to have reached as high as the Valhalla to the south (Norlander 1982). Deformation probably stopped at the same time as the Valhalla dome (Gordon et al. 2008).

The Frenchman Cap dome lies in between the Thor-Odin and the Malton domes. Like the previously mentioned domes it contains E-W lineations (Gervais et al. 2010). Deformation is thought to have begun around 60-55 Ma, which is slightly later than the other two domes (Gervais et al. 2010). Specific temperatures were not mentioned, but the lower cover contains sillimanite, which is stable at high temperatures, and the upper cover contains kyanite, which is stable at high pressures (Gervais et al. 2010). This indicates the Frenchman Cap, like the others, experienced amphibolite facies metamorphism (Gervais et al. 2010). It is also said to have experienced cooling and exhumation at the same time as other domes within the SMCC (Gordon 2008).

5. Structural Observations from the Malton Dome

There are significant spatial differences in the kinematics of deformation at different structural depths within the Malton Dome (Robinson and Sisson 2011). At shallower structural levels along the northern tip of the Malton Dome and the southernmost end immediately beneath the Monashee Decollement, stretching lineations trend EW corresponding with the rest of the SMCC (Morrison 1982). At deeper structural levels, lineations trend NW-SE (Fig 9) (McDonough and Simony 1989, Cowgill 1994). These rocks, which are the focus of my thesis, are thought to have obtained their ductile deformation fabrics during prograde metamorphism within the dome (McDonough and Simony 1989). This is interpreted to have been an earlier deformation period which is overprinted by the EW lineations observed at the northern tip (Robinson and Sisson 2011). This indicates that the upper and lower structures were detached from each other by the Monashee Decollement (Brown et al. 1986).

Structurally overlying the Malton Dome is the Monashee decollement (Fig 2), an ENE verging shear zone thought to be a continuation of the Rocky Mountain Fold and Thrust basal decollement (Cook et al. 1988, Brown et al. 1986). The decollement accommodated decoupling of the cover Mica Creek succession from the gneisses below, and is thought to have been the primary structure accommodating eastward movement of the hinterland (Brown et al. 1986).

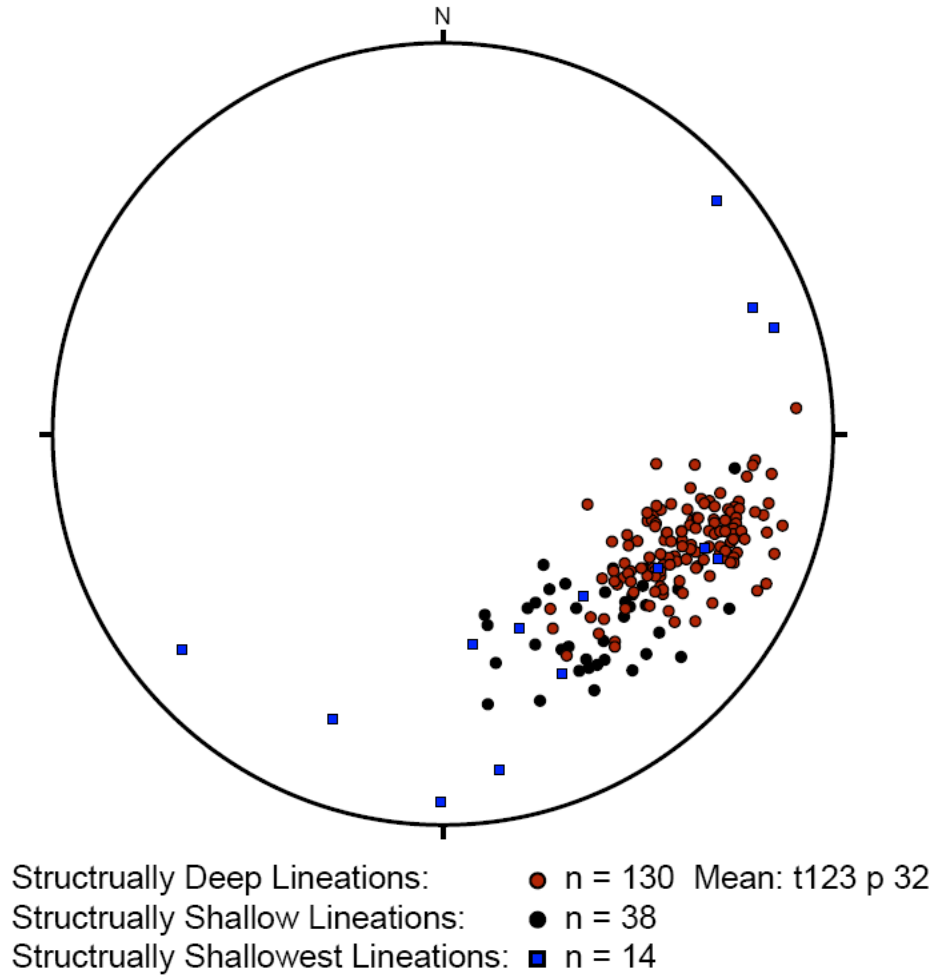

Fig 9: Lineations from the Malton Gneiss Dome, trending NW-SE as shown by Cowgill 1994

6. Tectonically Forced Orogen Parallel Flow

Tectonically forced orogen parallel flow occurs when channel flow of mid to lower crust reaches a barrier causing flow to move laterally, parallel to the orogenic front. Most of the rocks throughout the SMCC record orogen perpendicular crustal flow (Brown et al. 1986, Monger and Price 2002), but there is a shift from orogen perpendicular to NW orogen parallel flow (Fig 8) within the Malton Dome

(McDonough and Simony 1988). The switch in movement is thought to have occurred due to an obstruction of flow from an area with either a structural or thermal boundary (McDonough and Simony 1988, Hatcher and Merschat 2006).

The Malton dome is located closest to the foreland (Fig 6) relative to the rest of domes within the SMCC, and may be the reason for why it displays orogen parallel deformation, marking the transition from orogen perpendicular to orogen parallel flow (McDonough and Simony 1988, Robinson and Sisson 2011). The obstruction altering flow direction is thought to be due to rocks moving up a ramp, and encounter lower pressures and temperatures, decreasing viscosity and hindering ductile deformation. With continued movement in the hinterland, the rocks in the front of the channelized flow are forced to move laterally to accommodate this movement. This model predicts that orogen parallel flow is coeval with regional peak metamorphism and migmatization in the SMCC

7. Methods

The goal of my study was to assess the possible link between peak metamorphism and deformation using quantitative thermobarometry and petrofabric observations. My methods for data collection are as follows

7.1 Electron Microprobe

Quantitative compositional analyses were carried out on a four spectrometer Cameca SX50 electron microprobe at both the University of Houston and Texas A&M

University. All quantitative work employed wavelength-dispersive spectrometers (WDS). Qualitative EDS analyses (spectra), at Texas A&M were obtained with an Imix Princeton Gamma Tech (PGT) energy dispersive system (EDS) using an ultra-thin window detector. The reduction scheme was PAP (Pichou and Pichoir, 1991) The University of Houston used SAMx software, and TAMU used Probe for Windows for analysis and data reductions.

Four samples, out of over a hundred, were chosen to be analyzed with the electron microprobe; 62910, 109.2, 97.2, and 106.1 (Table 2) (Fig 2). Analyses were performed on multiple mineral phases to calculate the peak metamorphic temperatures and pressure the rocks experienced within the Malton. These minerals included: garnet, feldspar, mica, and amphibole. All samples contain garnet, and the majority of the matrix minerals were analyzed as close to the garnet as possible. Care was taken as well to analyze both other garnet grains and matrix minerals in the sample to make sure there was no significant variation in composition between like minerals in order to address whether the sample had achieved equilibrium.

7.2 Garnet Analysis

The standards that were used to test the weight percent of the 6 major elements within garnet were as follows: Quartz for Si; Corundum for Al, Diopside 15 for Ca; Garnet 13 for Fe, Rhodinite for Mn; and MgF for Mg. O was calculated using

the stochiometry formula for each mineral. These standards were placed into a run file and tested against the garnet-13 standard, with an error of ±5% for weight %

Sample Name	Location	Mineralogy	Kinematic indicators &Micro fabrics
62910	Middle/Northern Malton Dome	Schist: staurolite, garnet, muscovite, biotite, quartz, and inclusions of tourmaline	GBM qtz deform; s-c fabric showing a top to the left sense of shear; porphyroblasts strain shadows showing top to the left sense of shear; inclusions indicating a counterclockwise rotation or top to the left sense of shear; mode 1 fractures confirming the s1 stress direction
1092	Southern portion of the Malton Dome, near the Monashee Decollement	Amphibolite: garnet, plagioclase, amphibole, biotite, quartz, scapolite	GBM qtz deform, with SGR; no kinematic indicators
97.2	Southern portion of the Malton Dome, near the Monashee Decollement	Amphibolite: garnet (many big chlorite), amphibole, epidote, biotite, quartz, plagioclase	GBM qtz deform, w/pos SGR; some qtz porphyroblasts may indicate some left lateral sense of shear
106.1	Southern portion of the Malton Dome, near the Monashee Decollement	Amphibolite: biotite amphibole, garnet, quartz, plagioclase	GBM qtz deform; s-c fabric showing left lateral sense of shear; porphyroblasts have left lateral sense of shear,

GBM= grain boundary migration, SGR= sub-grain rotation

Table 2: Summary of analyzed samples for this study area

between 10 and 30, and ±2% for anything greater than 30 weight %. These errors were used for all of the other minerals analyzed. Once the standards were verified as being accurate, my samples were analyzed using a beam of 20Å, and a size of 10μm.

Garnet composition profiles were taken within each sample with at least 20 points per profile, divided evenly across the garnet (Fig 10). Inclusions or altered areas within the garnet were often encountered, if a cleaner spot was within 5 μm, then the point was taken there, otherwise the spot was analyzed and noted as being potentially bad data and removed from the composition profiles. In the case of sample 109.2 an inclusion in the middle of the garnet was so large that the profile was split up into two separate portions.

X-ray maps were obtained at 15kV and a 50nÅ beam, 1μm in size. Points were taken every 4μm, and every 15 ms. There were 7 elements measured; Mg, Si, Ca, Fe, Na, Al, Ti and Mn.

7.3 Feldspar Analysis

Five major elements were analyzed in the feldspars: Na, Ca, Al, Si, and K. The standardizations were as follows: Jadite for Na, Anorthite for Al (EDS), Anorthite for Si (EDS), Microcline for K, and Anorthite for Ca (WDS). Once standardization was complete it was tested against microcline.

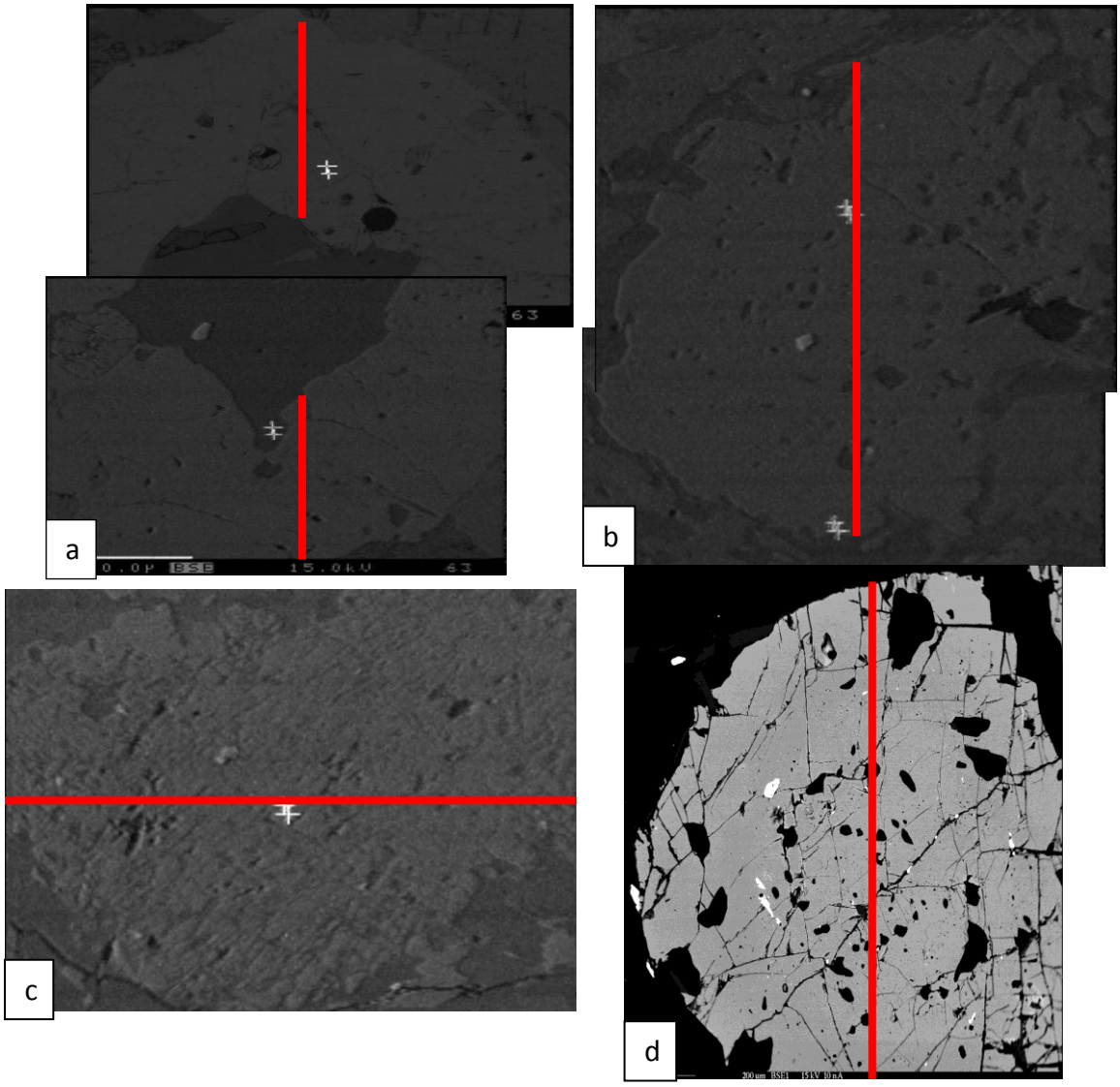

Fig 10: BSE images of the garnet profile paths, indicated by the red line, for a)1092, b)1061, c)972, d)62910

7.4 Amphibole & Mica Analysis

Amphibole and mica analysis were performed at Texas A&M University. Twelve elements were standardized and tested for both minerals within my samples The standardizations were as follows: Phlogopite for F, Albite for Na, Diopside for Mg & Si, orthoclase for Al, Ca & K, NaCl for Cl, Ilmenite for Ti, Olivine for Fe, Spessartine for Mn, and Chromite for Cr. Amphibole standards were tested against both Kakanuie hornblende and Arenal hornblende.

7.5 Geothermometry and Geobarometry

Multiple geothermometers and geobarometers were used to calculate estimates in temperature and pressure for the four samples. There was one geobarometer used; garnet/plagioclase/hornblende (gphb), with the following reactions being used for calculations:

1) 12fact+21ts+42ab=22gr+20alm+21gl+54q (Holland & Powell 1998) (gphb 972)

2) 7ts+3ab=3py+3parg+8an+8q+H_2O, (gphb1092)

3) 39fact+84ts+63ab=40gr+65alm+63parg+312q+60H_2O (gphb 1061)

There were also three geothermometers used; garnet/hornblende (ghb), garnet/biotite (gb) and hornblende/plagioclase (hbp) with the reactions for each as follows:

1) 6fact+60parg+80q=20gr+10alm+21tr+15ts+30gl (972 ghb)

2) 5py+3fact=5alm+3tr (ghb 1092)

3) 5py+3fact=5alm+3tr (ghb 1061)

4) py+ann=alm+phl (gb 1061 & 62910)

Three out of the four geothermometers/barometers were calculated using THERMOCLAC v 3.33 and the thermodynamic database of Holland and Powell (2003), including garnet/plagioclase/hornblende, garnet/hornblende, and garnet/biotite. The hornblende/plagioclase thermometer was calculated using HB-PLAG (Holland, 2003).

There are certain problems that may arise within testing for certain phases. For example, if garnet and biotite deviate from their ideal Fe-Mg binary system this may lead to inaccurate temperature estimates (Ghent et al. 1982). Caution also has to be taken with respect to garnet zonation, which can be altered at higher grade metamorphism, or during retrograde reactions (Ghent et al. 1982). I also have to consider retrograde net transfer reactions, as they can change the composition of the minerals within the samples and affect P-T conditions (Kohn and Spear 2000). Finally, minerals may not be in equilibrium with each other and therefore not recording peak metamorphic conditions, especially in regard to biotite (Henry et al. 2005).

8. Results

8.1 P-T conditions

P-T graphs were created by plotting values calculated by THERMOCALC for separate reactions that occurred within each sample. Average P-T conditions were

also calculated using THERMOCALC, which were plotted both on the graphs for the respective samples, as well as a graph with all of the average P-T calculations and standard deviation. Reported temperatures and pressures represent ranges calculated by multiple reactions from THERMOCALC.

Sample 972, located in the southern portion of the Malton dome, is an amphibolite composed of garnet, amphibole, biotite, quartz, plagioclase, and some epidote. The garnet within the sample are highly chloritized, and are remarkable in that they contain little to no pyrope (Mg) end-member. The garnet that was analyzed produced some outlying values when calculating oxides. These extraneous values were excluded when graphing the profiles. The garnet profile for 972 was taken across a 1792 μm garnet (Fig 11a). The plot shows that the garnet is predominantly composed of almandine (Fe) end-member of garnet. Figure 11 shows that all elements have a relatively flat profiles (once the chlorite values were removed) indicating that the garnet may have been affected by retrograde metamorphism. There are a lot of missing points within the 972 profile, due to the heavily chloritized nature of the garnet. I interpret that the profile is indeed flat, like the other samples, because of the points that were unaltered were all essentially similar in composition. The presence of epidote along with chlorite within sample 972, also indicates that it has experienced retrograde metamorphism (Guynn et al. 2013).

a)

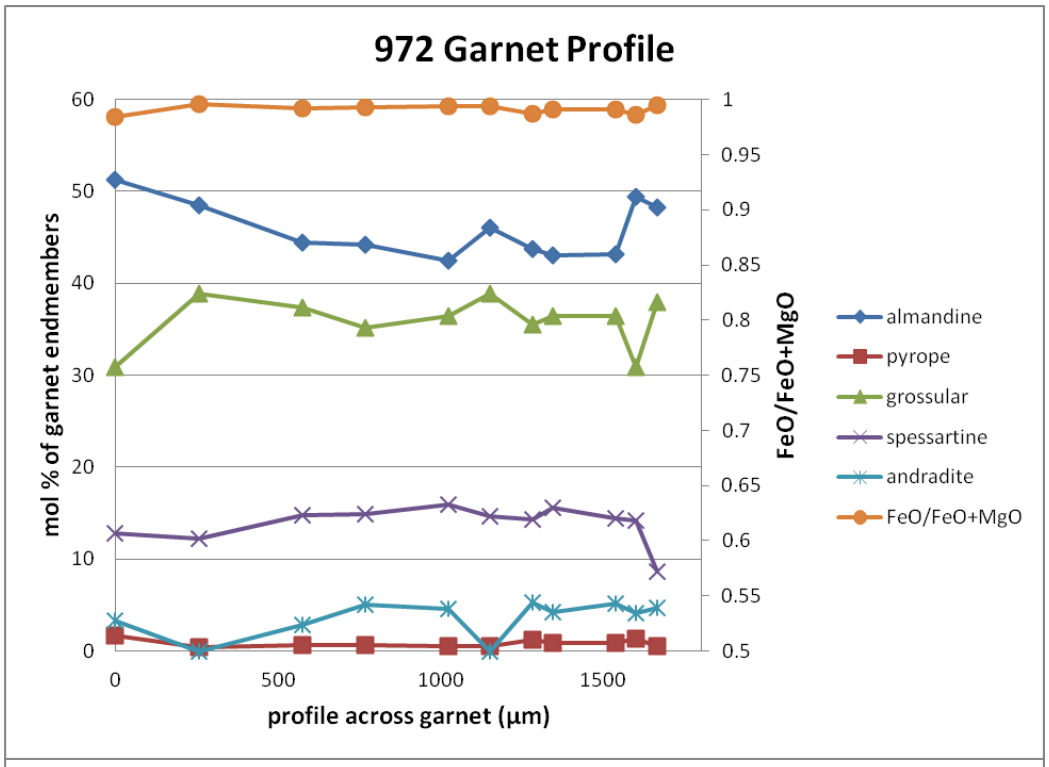

b)

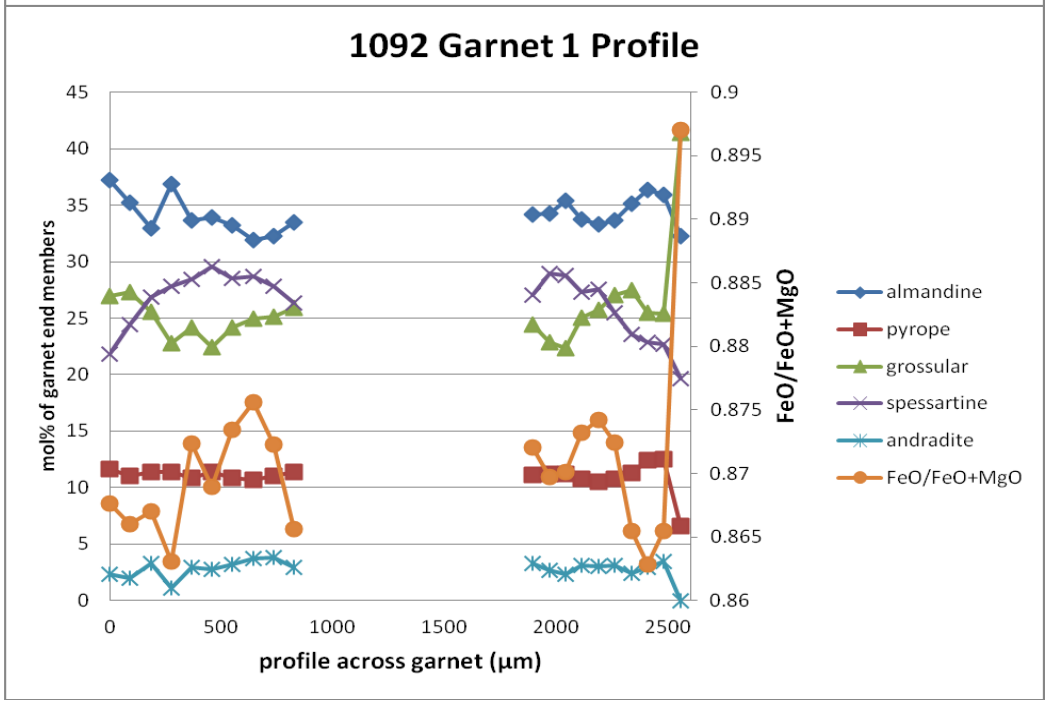

Fig 11: Garnet end member profiles made for the 4 samples analyzed for P-T conditions, a)972, b)1092, c)1061, d)62910.

c)

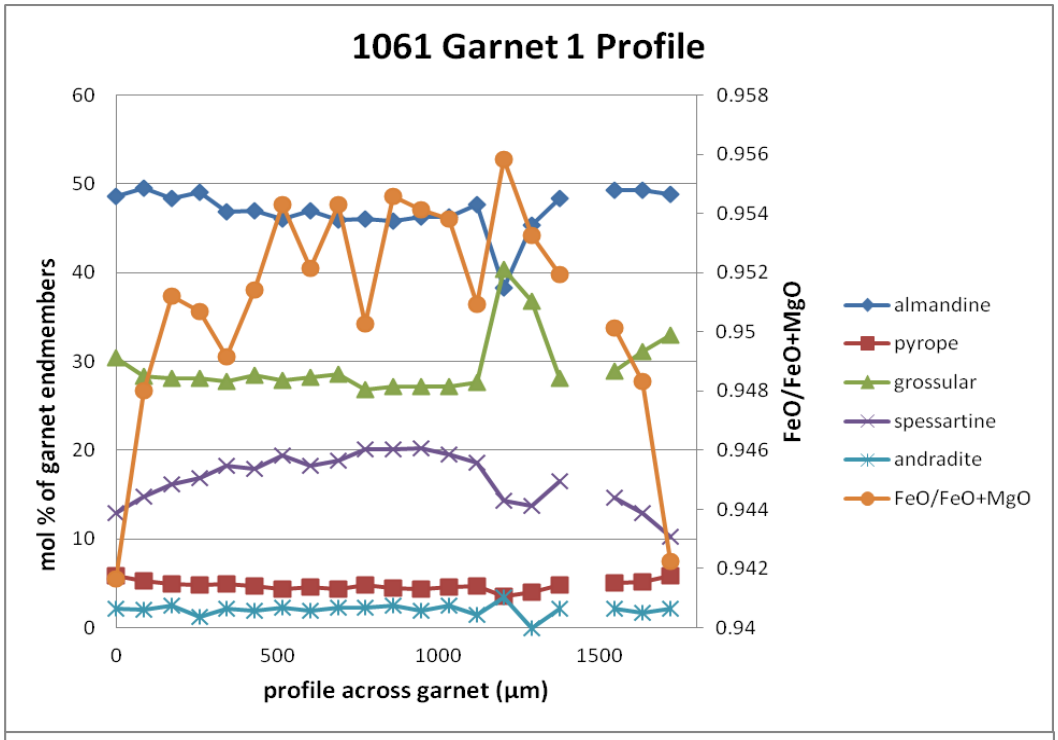

d)

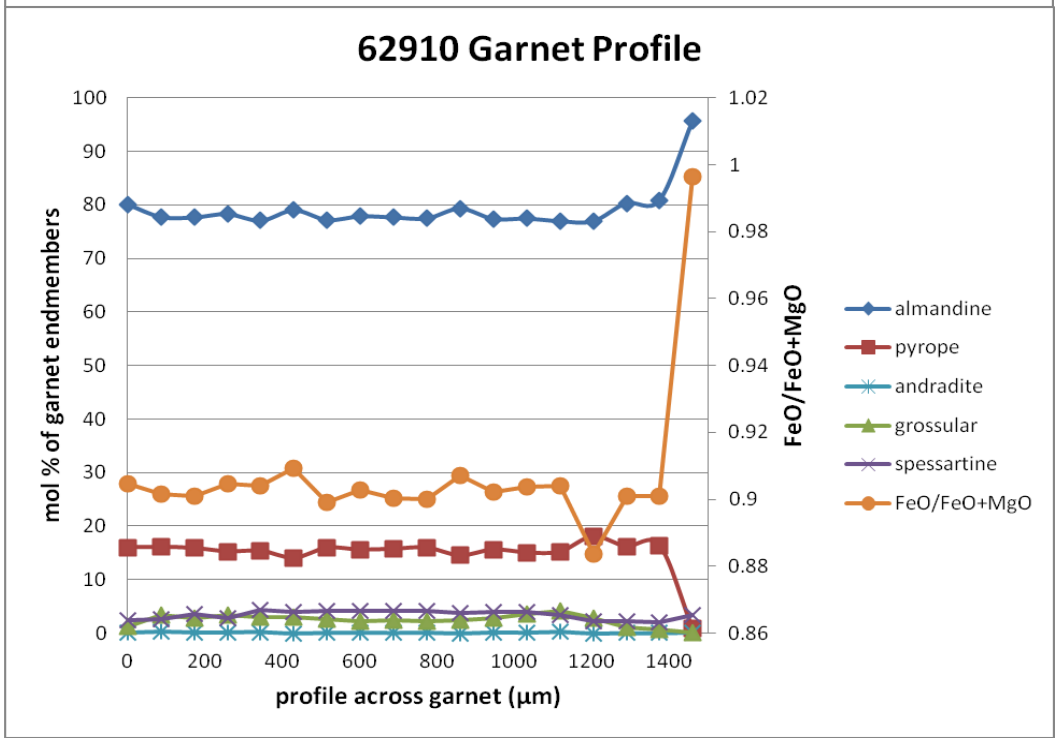

Fig 11: Garnet end member profiles made for the 4 samples analyzed for P-T conditions, a)972, b)1092, c)1061, d)62910.

Along with the end-member plots there were three thermometers and barometers calculated with THERMOCALC. Garnet/plagioclase/hornblende yielded P-T conditions of 301-525 MPa and 600-800 ^{0}C. The hornblende/plagioclase thermometer produced temperatures of 727-706 ^{0}C. The Garnet/hornblende reaction produced a range of P-T conditions from 300-700 MPa and 475-750 ^{0}C. Although there was biotite within the sample no reactions for the garnet biotite geothermometer were returned by THERMOCALC, likely due to the lack of pyrope within the garnet. The average P-T calculated was 1192 MPa and 775 ^{0}C. All of these calculations place sample 972 at amphibolite facies conditions (Fig 12a). However the average pressures are inconsistent with other results and other regional P-T studies. Pressure conditions were calculated using the average of the separate reactions measured for the sample, which yielded a pressure of about 415 MPa.

Sample 1092 is located in the southern portion of the Malton dome. It is an amphibolite, composed of garnet, plagioclase, amphibole, biotite, quartz, and scapolite. The garnet profile for this sample was taken from a 14584 μm wide garnet, which had a 1070 μm plagioclase inclusion within the middle (Fig 11b). This inclusion is represented by the large gap in the profile. Spessartine (Mn) end-member, and grossular, the Ca rich end-member, have an inverse relationship with each other. This relationship may be related to the plagioclase inclusion within the garnet, but is most likely showing some preservation of growth zoning. The increase in Ca within the core is typically seen when growth zoning was present (Caddick et

a)

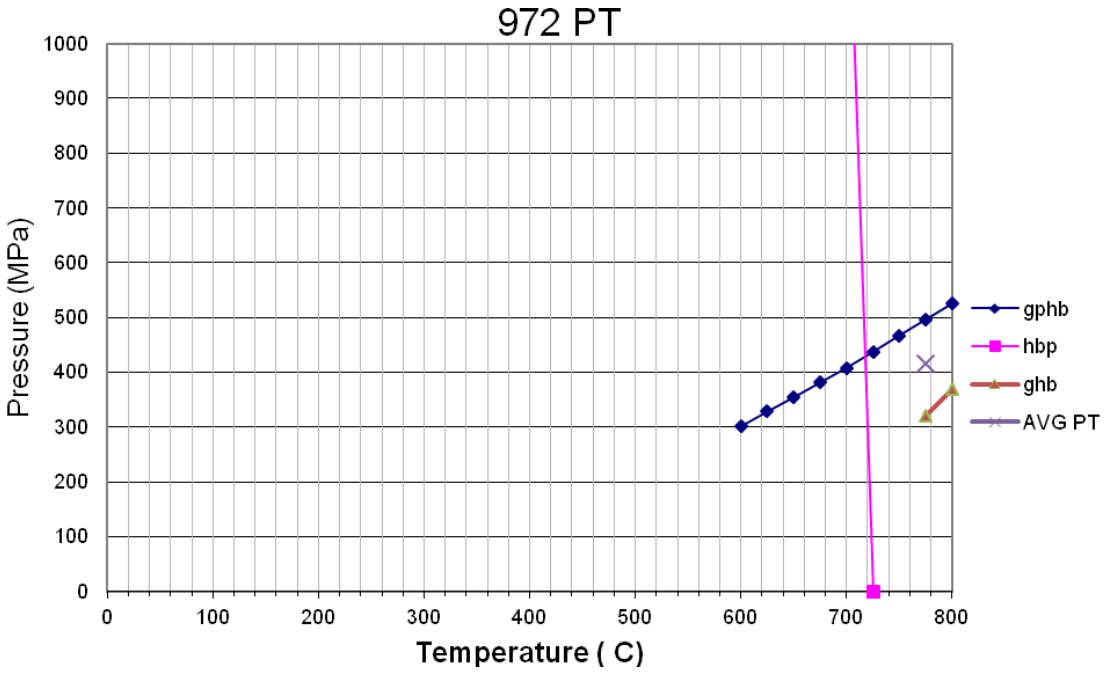

b)

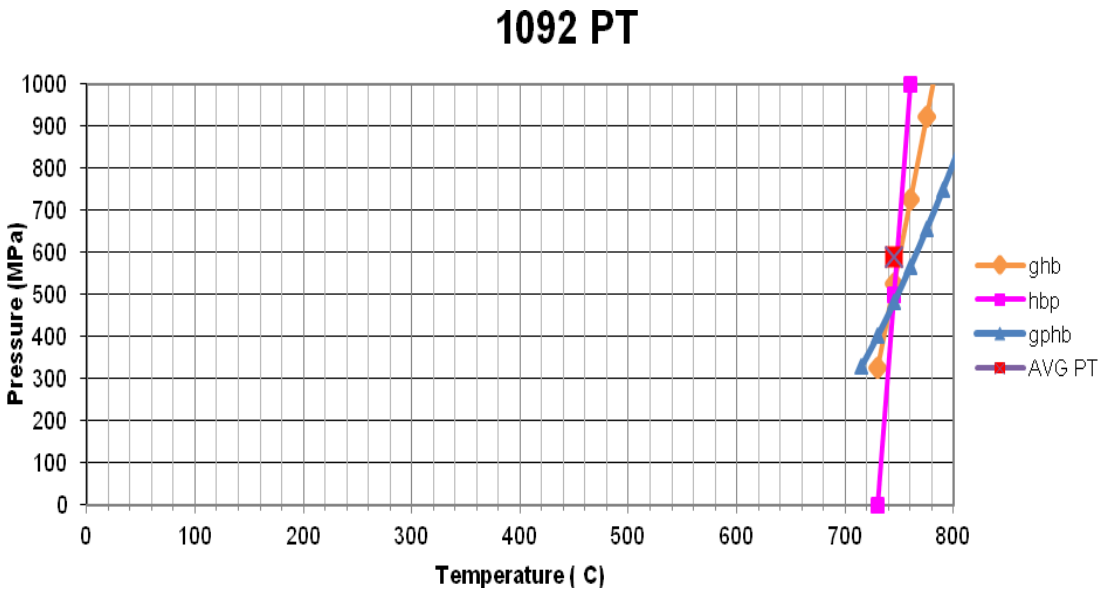

Fig 12: P-T graphs for each geothermometer and geobarometer that was measured for each sample, a)972, b)1092, c)1061, d)62910

c)

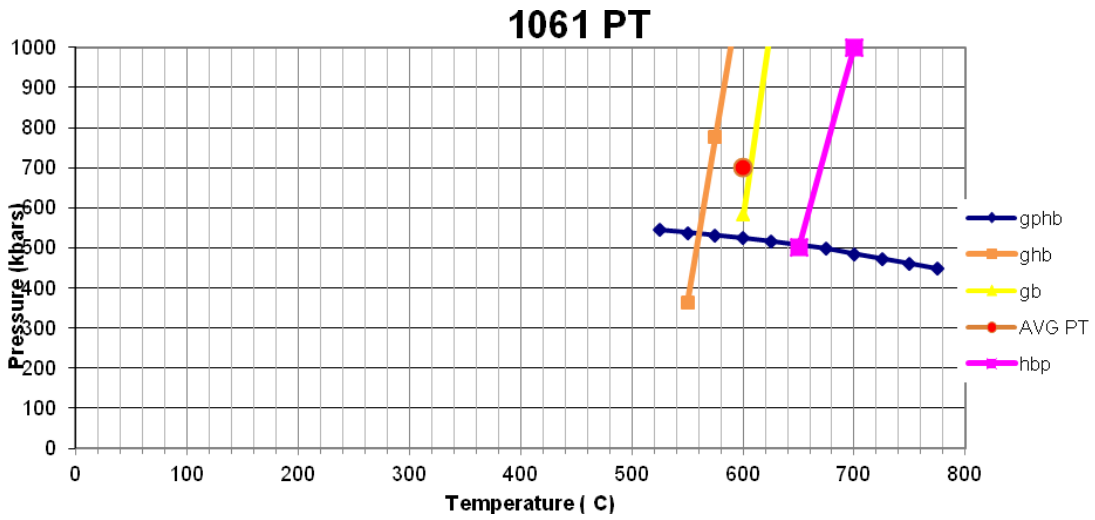

d)

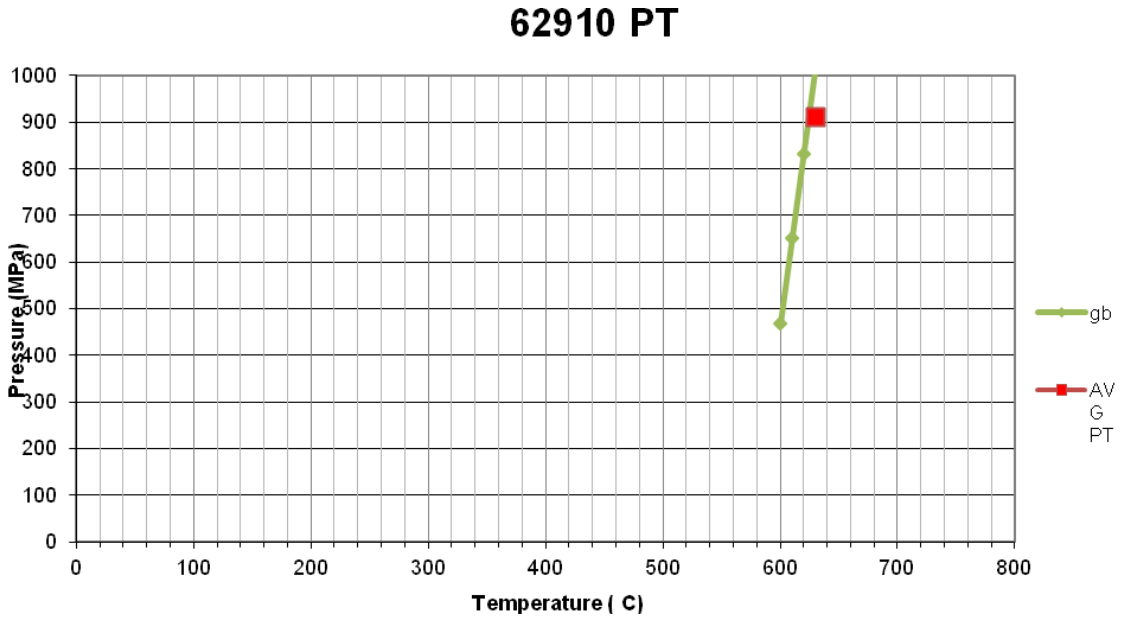

Fig 12: P-T graphs for each geothermometer and geobarometer that was measured for each sample, a)972, b)1092, c)1061, d)62910

al. 2010). The other end member concentration profiles are relatively flat with a slightly higher concentration of FeO/FeO+MgO in the core.

Three geothermometers and geobarometers were able to be used for P-T estimates (Fig 12b). The garnet/hornblende geothermometer gave a temperature range of 728-796 ^{0}C. The hornblende/plagioclase geothermometer yielded temperatures of 732-768 ^{0}C. Finally, the garnet/plagioclase/hornblende reaction yielded temperatures of 715-850^{0}C. The average P-T calculated was 590MPa and 745^{0}C.

Another sample taken from the same outcrop, sample 1092:8-1, contained kyanite. This indicates that the samples would have to have been in the kyanite zone. Average P-T calculations for 1092 do overlap this zone within uncertainty, which indicates that it was in the kyanite zone with slightly lower temperatures and higher pressures than the values calculated by THERMOCALC. This is beneficial, because it significantly narrows the P-T window which the samples experienced, because most results have plotted in the sillimanite stability field (Fig 13).

Sample 1061 is the southernmost sample within the Malton dome, near sample 972. 1061 is an amphibolite, which contains garnet, amphibole, plagioclase, quartz, and biotite. A garnet profile was taken across a 1720 μm garnet (Fig 11c). Four out of the five garnet end members measured remain relatively consistent and flat, with very slight zoning in pyrope and almandine, from core to rim. The significant difference is within the Spessartine (Mn) end member, which has a

higher concentration in the core than within the rim. This pattern is also noticed for the FeO/FeO+MgO.

An X-ray composition map of a garnet from sample 106.1 was also made , for four important cations; Fe, Ca, Mg, and Mn. (Fig 14). There is little to no variation between the core and rim, except in the case of Mn where there is a higher concentration within the core than in the rim. This observation corresponds to what was seen in the zoning profile. With the correlation between the x-ray and the

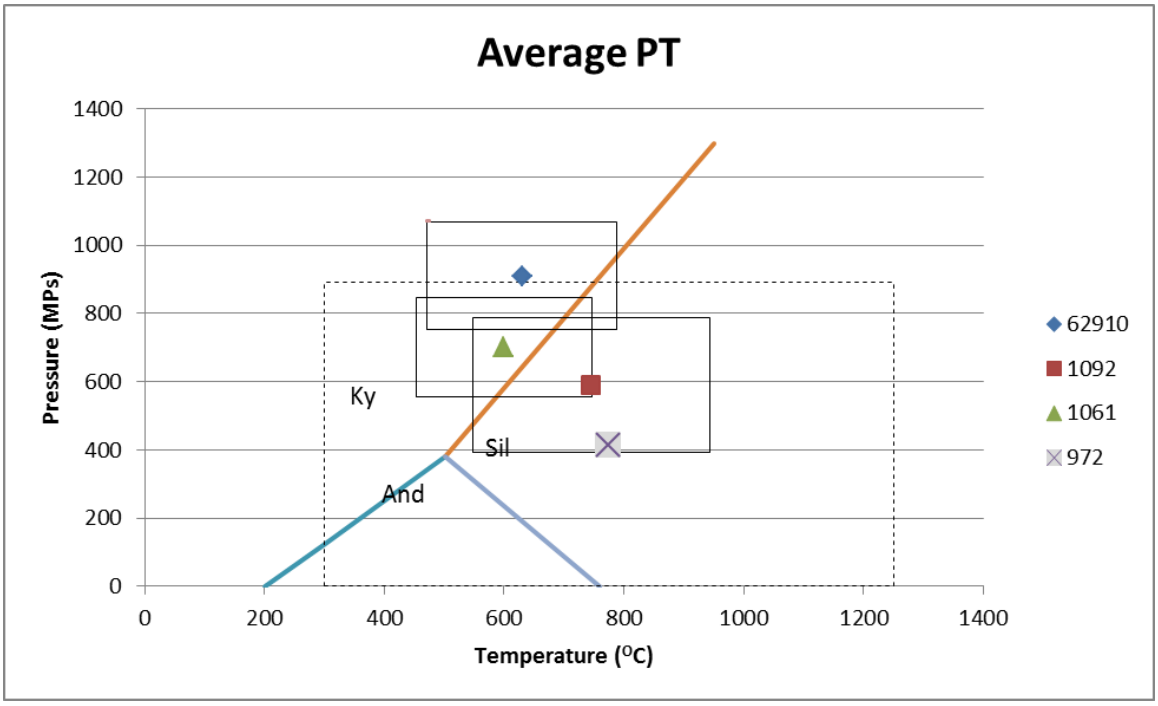

Fig 13: Calculated average P-T for the 4 samples. Black boxes indicate standard deviation, dotted box is for sample 972 which has an estimated standard deviation as well as an estimated pressure. Graph also show the Kyanite, Sillimanite, Andradite zones

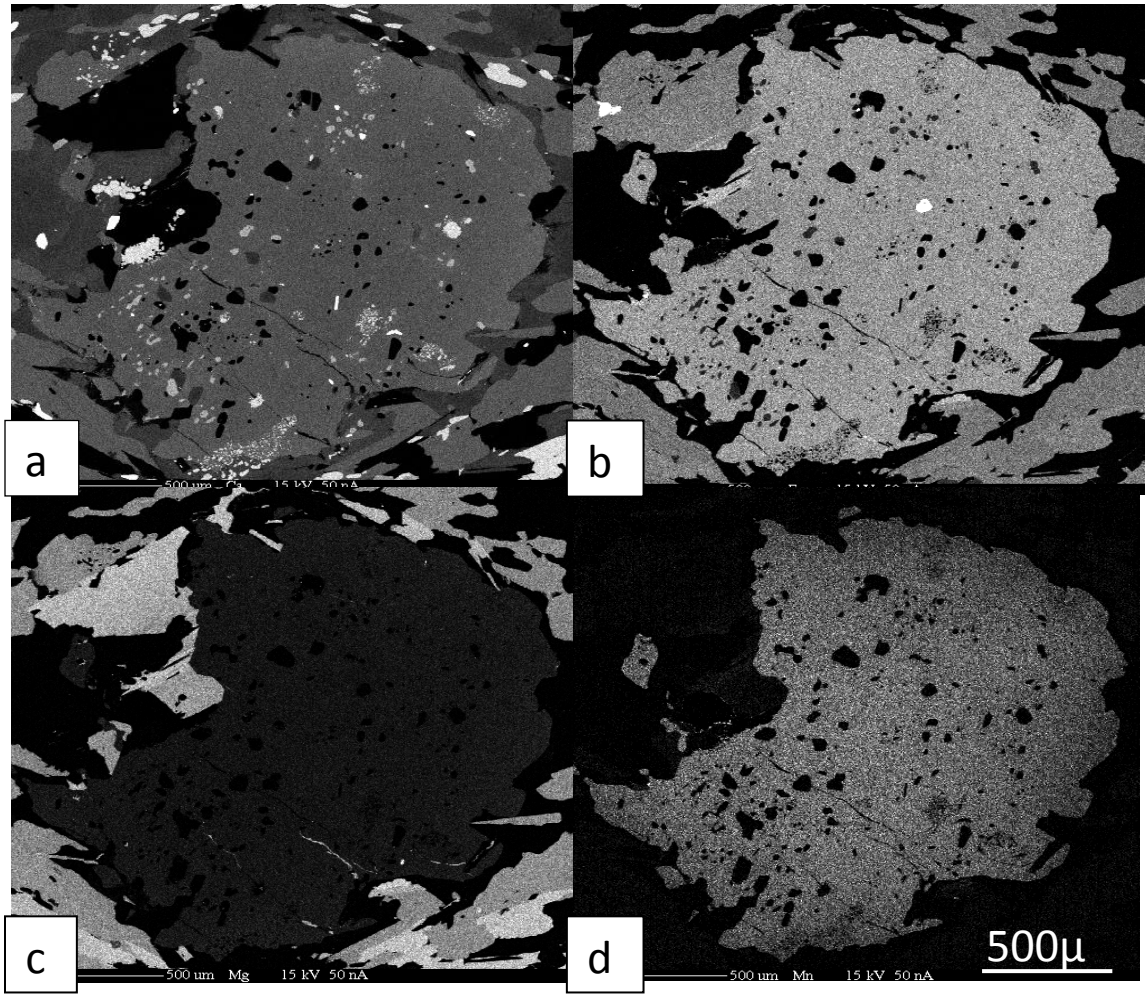

Fig 14) X-ray garnet composition maps from sample 1061 for, a)Ca, b)Fe, c)Mg, d)Mn. The lighter the area the higher the concentration of that element.

garnet profile of 1061, it can be assumed that the other garnet profiles are adequate representations of the profiles of the garnet grains within the samples.

Four geothermometers and geobarometers were used based on analyses from sample 1061(Fig 12c). Estimations for garnet/hornblende yielded temperatures of 728-796 ^{0}C. The hornblende/plagioclase geothermometer yielded temperatures of 644-727 ^{0}C. The garnet/biotite geothermometer returned temperature ranges of 585-634 ^{0}C. Finally, the garnet/plagioclase/hornblende geobarometer, produced a range of 400-1100 MPa and 597-722 ^{0}C. The average P-T estimated by THERMOCALC was 700 MPa and 600 ^{0}C. This places the sample within the middle amphibolite metamorphic facies.

Sample 62910 is the furthest north of the four analyzed. It is a pelitic schist that contains staurolite, garnet, muscovite, biotite, quartz and inclusions of tourmaline. A garnet profile was taken across a 1460 μm garnet (Fig 11d). The profiles of the end-members show little to no variation from the core to the rim, which indicates the garnet was diffusionally homogenized during peak metamorphic conditions, which may be an indication that this sample hasn't experienced any retrograde reactions. There was only one geothermometer, garnet/biotite, used for 62910 due to its composition (Fig 12d), and a temperature range of 600-650 ^{0}C was calculated. An average P-T was also calculated using THERMOCALC, which returned values of 910 MPa and 630 ^{0}C. A relatively close sample 7610.3 located to the north, contained both kyanite and sillimanite, indicating that these samples experienced P-T

conditions between 700-800 ^{O}C , and 750-950 MPa, on the kyanite sillimanite boundary. This means the pressures were probably towards the lower limits within the standard deviation for 62910, if the temperature calculated is correct. Values and observations place sample 62910 in the amphibolite metamorphic facies.

8.2 Petrofabric Observations

The four samples analyzed for PT conditions were also examined for significant petrofabric indicators, such as strain shadows around porphyroblasts, s-c fabrics, inclusion paths, and quartz deformation fabrics. The three samples in the south didn't contain significant of kinematic indicators compared to sample 62910 in the north.

Sample 62910, the furthest north sample contained several kinematic indicators including syn-kinematic garnet and feldspar porphyroblasts (Fig 15a). Porphyroblasts contain many inclusions, some seeming to preserve a previous fabric, while others have spiral inclusions with kinematics consistent with the S-C fabrics (Fig 15c).These syn-kinematic porphyroblasts have strain shadows containing muscovite, biotite, and quartz. 62910 also has an s-c fabric within the micas that also shows a left lateral sense of shear within the slide(Fig 15b). In addition to these kinematic indicators 62910 also displays grain boundary migration quartz deformation fabric(GBM), which indicates temperatures in the 500-700 ^{O}C range (Passchier & Trouw 2005).

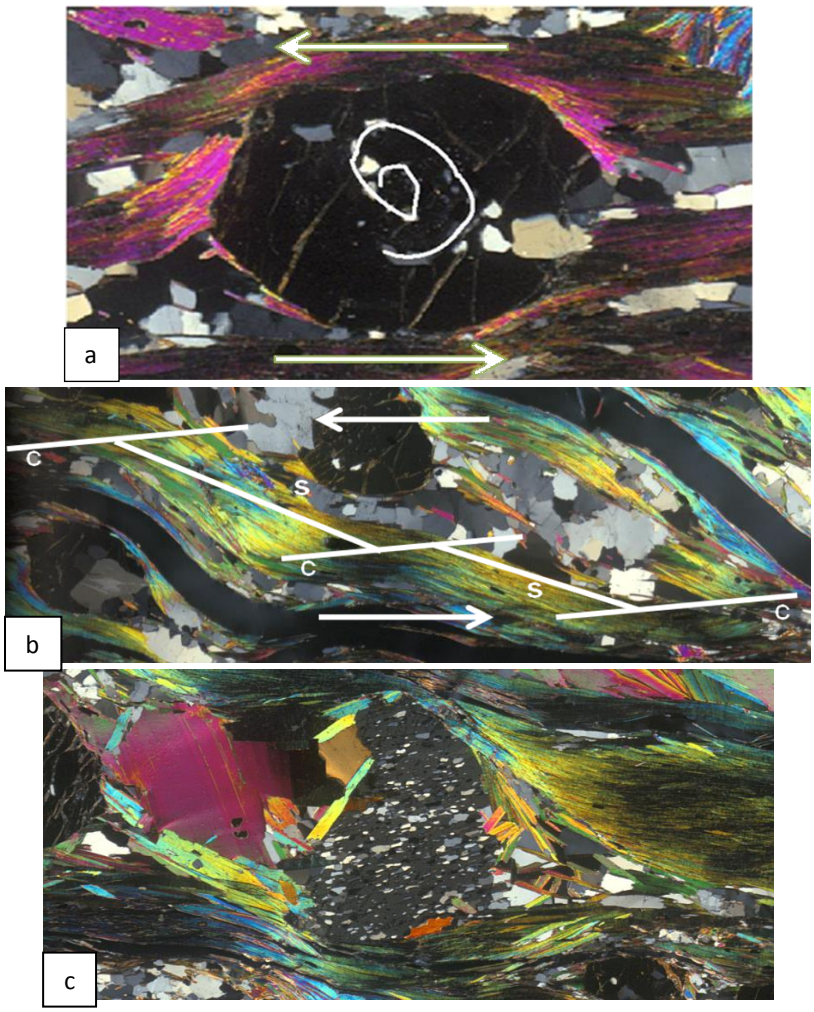

Fig 15) All images from sample 62910. a) is and syn-kinematic porphyroblast that includes spiral inclusions, b) s-c fabric, c) a garnet porphyroblast which preserves a previous fabric.

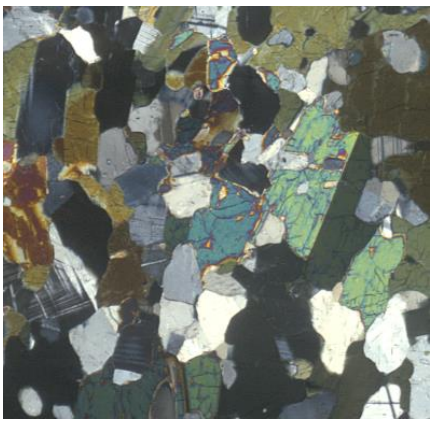

Fig 16: Grain boundary migration (GBM) quartz deformation fabric for sample 1092

Sample 1092 does not contain deformation fabrics useful for evaluating PT or shear sense within the sample, other than quartz deformation fabrics showing grain boundary migration (Fig 16).

Sample 972 contains a syn-kinematic feldspar porphyroblasts with strain shadows predominantly composed of biotite that have since been overprinted by retrogradation (Fig 17a). Quartz deformation fabrics within sample 972 include both GBM and SGR (Fig 17b). The presence of sub grain rotation suggests that the sample continued to deform after peak P-T conditions, documented by GBM.

Finally sample 1061, the furthest south of the four samples, contains a couple different kinematic indicators. The garnet located at the edge of the slide have strain shadows composed of both amphibole and biotite. As well as the porphyroblasts, there is an s-c fabric with the same sense of shear. The quartz deformation fabrics displayed both GBM and SGR (Fig 18a), like 972. The garnet also contains numerous inclusions, which preserve a previous foliation within the matrix (Fig 18b).

9. Discussion

9.1 P-T data

The average P-T graph shows that all of the calculated P-T conditions are within the same range (Fig 13), within the middle to upper amphibolite facies. Based on the results, I interpret samples 1061 and 1092 to have essentially the same P-T conditions, especially when considering the sample from the same outcrop

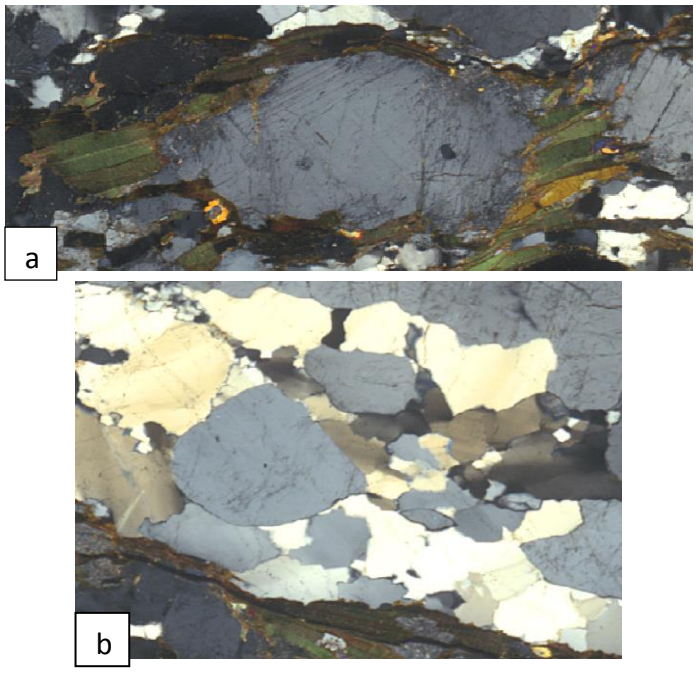

Fig 17: Petrofabric observations for sample 972 a) since altered quartz porphyroblast, that seems to have been syn-kinematic, b) GBM & SGR quartz deformation fabrics

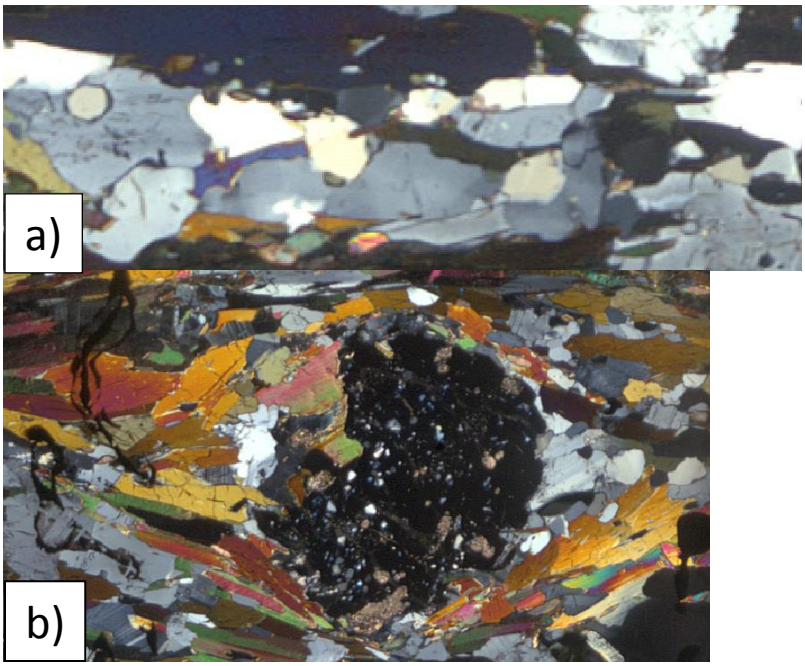

Fig 18: Petrofabric observations for sample 1061, a) contains GBM & SGR, b) preserved previous fabric within the porphyroblast.

as 1092 contains kyanite. This may indicate that the entire dome experienced similar conditions. The average P-T calculated for sample 972 has the highest P values compared to all of the samples, but it also has the largest error, compared to the other three samples. This may be due to the fact that some of the minerals are no longer in equilibrium with each other, and are showing retrograde reactions, as mentioned earlier with the issues with the garnet profile. Based on the results falling in the amphibolite facies, and the lack of clinopyroxene or orthopyroxene, that metamorphism never reached the granulite facies (Morrison 1982). These estimations are further confirmed by PT work performed by Morrison which yielded amphibolite facies in the Malton Dome.

The x-ray composition map of the garnet within sample 1061 supports my interpretation that it reached high metamorphic conditions, due to the fact that there is no significant variation of elements from rim to core (Fig 14). The entire garnet is interpreted to have been diffusionally homogenized.

The consistent observation of GBM and SGR within the quartz indicates that the samples were under high temperatures, from about 500 to slightly over 700 ^{O}C, which further corresponds to the temperatures estimated for these samples (Passchier & Trouw 2005).

9.2 Petrofabric observations

There were multiple kinematic indicators within the samples as discussed above. The three samples with kinematic indicators were used to be able to connect deformation with peak metamorphic conditions. The porphyroblasts within some of samples were syn-kinematic, and tied deformation to peak metamorphism. Both the garnet porphyroblasts and the deformed matrix around them, which made up the strain shadows, were assumed to be in equilibrium with each other, as well as with the rest of the sample. So, the minerals that make up the kinematic indicators also preserve peak metamorphic conditions. This fulfills one of the requirements needed for the tectonically forced orogen parallel flow, the proposed model of ductile deformation within the Malton dome.

Looking at the location of the samples, 62910 in the north and the other three in the south, there are some conclusions that can be made. Due to the observation that all samples return values within the amphibolite facies indicates the entire dome may have reached similar peak metamorphic conditions. Also, when looking at the plot of average P-T if you exclude 972, which was probably altered as mentioned, the highest P-T is in the north, with the other two samples further south yielding similar lower values. Another possibility may be that the samples in the south experience some retrograde reactions. Clearly more P-T documentation are needed.

9.3 Regional Implications

As well as the shear sense being different in the Malton Dome, than in the other three domes, there seems to be very slight differences in the metamorphic conditions. Previous work in the Malton dome has documented amphibolite to upper-amphibolite facies, but the other gneiss domes of the SMCC have higher average temperatures place them at having temperatures than the Malton, with temperatures in the mid 800's, for the Valhalla Dome (Carr and Simony 2006). The Valhalla seems to have the highest reported temperatures, and they decrease towards the north, which would fit with the Malton having the lowest metamorphic temperatures. This pattern of a gradual change from north to south is also seen in the age of initial deformation. The estimated dates for initial and peak metamorphic conditions get younger as you move northward, with the Valhalla having the oldest dates although they are not significantly different (Gordon et al. 2008). This pattern may have implications for the relative age of metamorphism within the Malton Dome, but no work has been performed on this yet.

Two cross sections were made (Fig 19a,b), one from the SW-NE, A-A', and the other from the NW-SE, B-B'. The thrust faults were assumed to have an angle of 30^{0}, unless known otherwise, and the normal faults were assumed to have an angle of 60^{0}, unless known otherwise (Anderson 1951). The cross section B-B' shows the four samples analyzed from essentially N-S. there seems to be no significant patterns within the P-T conditions for the samples, with exception to sample 62910

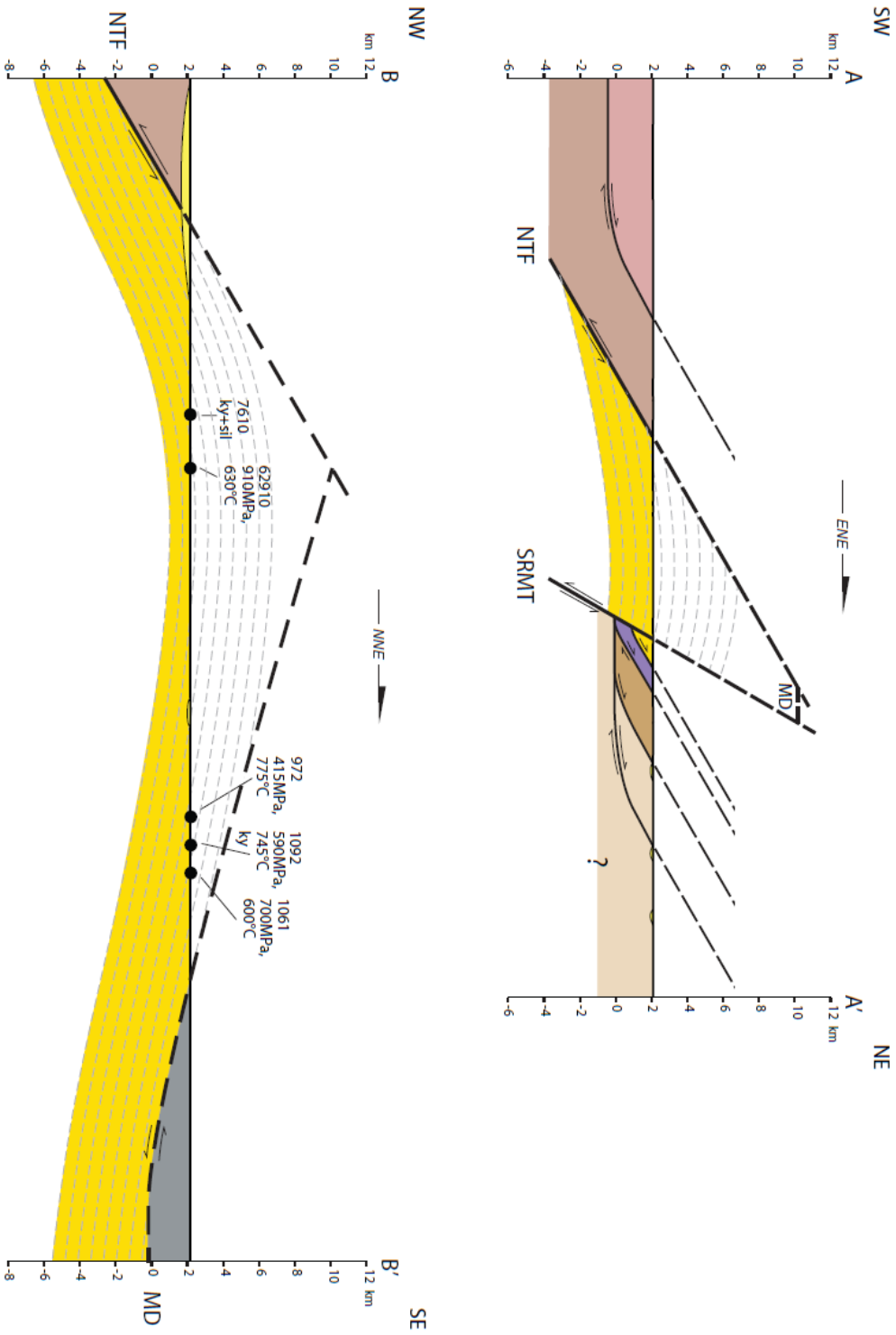

Fig 19: 2 cross sections made within the Malton Dome a) A-A' runs SW-NE, also shows the cross cutting relationship of the NTF, SRMT, and the MD, b) B-B' runs NW-SE and shows the samples relative to each other. NTF= North Thompson Fault, SRMT= Southern Rocky Mountain Trench, MD= Monashee Decollement.

yielding a significantly higher pressure, when considering the altered pressure for 972. The lack of pattern indicates that the presently exposed dome shows progressively deeper rocks to the north, with higher pressure results in 62910. This may also explain why the three southern samples seem to be experiencing some retrogradation, because they were structurally higher, and under lower pressures, they crossed back into a lower metamorphic facies and are displaying retrograde reactions.

10. Conclusions

1. PT calculations have returned temperatures and pressures within amphibolite to upper amphibolite facies metamorphism. These temperatures and pressures ranged from 600-775 ^{0}C, and 450-900 MPa.
2. Peak metamorphism and deformation are interpreted as being simultaneous, as porphyroblasts and their strain shadows have PT values corresponding to peak metamorphism. This fits with the forced orogen parallel flow model.
3. The cross sections fit the assumption that the entire Malton Dome experienced relatively the same peak metamorphic conditions. This is indicated by the only significant difference being within the pressure of the sample located the furthest north, 62910. This sample had a significantly higher pressure than the other samples, suggesting that it was structurally deeper.

Works Cited

Armstrong, R.L., 1982, Cordilleran Metamorphic Core Complexes, Annual Reviews Earth and Planetary Science, v. 10, p. 129-154

Bally, A. W., Gordy, P. L., Stewart, G. A., 1966, Structure, Seismic data, and Orogenic Evolution of Southern Canadian Rocky Mountains, Bulletin of Canadian Petroleum Geology, v. 14, n. 3

Beaumont, C., Jamieson, R. A., Nguyen, M. H., and Lee, B., 2001, Himalayan tectonics explained by extrusion of a low-viscosity crustal channel coupled to focused surface denudation: Nature, v. 414

Brown, R. L., Journeay, M., Lane, L. S., Murphy, D. C., Rees, C. J., 1986, Obduction, backfolding and piggyback thrusting in the metamorphic hinterland of the southeastern Canadian Cordillera, v. 8, n. ¾

Caddick, M.J., Konopasek, J., Thompson, A., 2010, Preservation of Garnet Growth Zoning and the Duration of Prograde Metamorphism, Journal of Petrology, v. 51, n. 11, p. 2327-2347

Carr, S. D., and Simony, P. S., 2006, Ductile thrusting versus channel flow in the southeastern Canadian Cordillera: evolution of a coherent crystalline thrust sheet, *in* Law, R. D., Searle, M. P., and Godin, L., eds., Channel Flow, Ductile Extrusion and Exhumation in Continental Collision Zones: London, Geological Society, London, Special Publication

Coney, P. A., and Harms, T. A., 1984, Cordilleran metamorphic core complexes: Cenozoic extensional relics of Mesozoic compression: Geology, v. 12

Cook, F. A., Green, A. G., Simony, P. S., Price, R. A., Parrish, R. R., Milkereit, B., Gordy, P. L.,Brown, R. L., Coflin, K. C., and Patenaude, C., 1988, Lithoprobe seismic reflection structure of the southeastern Canadian Cordillera: initial results: Tectonics, v. 7, p. 157-180.

Cowgill, E. S., 1994, Evolution of the basement-cover boundary above the Malton Gneiss, Southeastern British Columbia: Results from a negative test of existing models [M.S. thesis]: University of Washington

Gervais, F., Brown, R. L., and Crowley, J. L., 2010, Tectonic implications for a Cordilleran orogenic base in the Frenchman Cap dome, southeastern Canadian Cordillera: Journal of Structural Geology, v. 32

Ghent, E. D., Knitter, C. C., Raeside, R. P., and Stout, M. Z., 1982, Geothermometry and geobarometry of pelitic rocks, upper kyanite and sillimanite zones, Mica Creek area, British Columbia: Canadian Mineralogist, v. 20

Gordon, S. M., Whitney, D. L., Teyssier, C., Grove, M., and Dunlap, W. J., 2008, Timescales of migmatization, melt crystallization, and cooling in a Cordilleran gneiss dome: Valhalla complex, southeastern British Columbia: Tectonics, v. 27

Guynn, J., Tropper, P., Kapp, P., Gehrels, E., 2013, Metamorphism of the Ando Metamorphic Core Complex, Tibet: Implications for the Jurassic Tectonic Evolution of the Bangong Suture Zone, Journal of Metamorphic Geology

Hatcher, R. D., Merschat, A. J., 2006, The Appalachian Inner Piedmont: an exhumed strike-parallel tectonically forced orogenic channel, *in* Law, R. D., Searle, M. P., and Godin, L., eds., Channel Flow, Ductile Extrusion and Exhumation in Continental Collision Zones: London, Geological Society, London, Special Publication

Henry, D. J., Guidotti, C. V. and Thomson, J. A. (2005) The Ti-saturation surface for low-to-medium pressure metapelitic biotite: Implications for Geothermometry and Ti-substitution Mechanisms. American Mineralogist, 90, 316-328

Holland, T.J.B., Powell, R., 1998, An internally consistent thermodynamic data set for phases of petrologic interest, Journal of Metamorphic Geology, v. 16, p 309-643

Kohn, M. J., Spear, F., 2000, Retrograde net transfer reaction insurance for pressure-temperature estimates, Geology, v. 28, n. 12

McDonough, M. R., Simony, P. S., 1988, Structural evolution of basement gneisses and Hadrynian cover, Bulldog Creek area, Rocky Mountains, British Columbia, Canadian Journal of Earth Science, v. 25

McDonough, M. R., and Simony, P. S., 1989, Vaelmount strain zone: A dextral oblique slipthrust system linking the Rocky Mountain and Omineca belts of the southeastern Canadian Cordillera: Geology, v. 17

Monger, J., Price, R., 2002, The Canadian Cordillera: Geology and Tectonic Evolution, Canadian Society of Exploration Geophysicists Recorder, v. 17, i. February

Morrison, M. L., 1982, Structure and Petrology of the Malton Gneiss Complex, Thesis at the University of Calgary

Norlander, B. H., Whitney, D. L., Teyssier, C., and Vanderhaeghe, 2002, Partial melting and decompression melting of the Thor-Odin dome, Shuswap metamorphic core complex, Canadian Cordillera: Lithos, v. 61

Passchier, C.W., Trouw, R.A.J., Microtectonics, Springer Verlag. 2005. second edition

Pouchou, J.L., Pichoir, F., 1991, Electron Probe Quantitation, K. F. J. Heinrich, D. E. Newbury, eds., Plenum, New York, p. 31

Robinson, A. C., Sisson, V., 2011, The Malton Gneiss Dome: Investigating orogen parallel ductile deformation in the Canadian Cordillera hinterland, NSF proposal

Sevigny, J. H., Parrish, R. R., Donelick, R. A., and Ghent, E. D., 1990, Northern Monashee Mountains, Omineca Crystalline Belt, British Columbia: Timing of metamorphism, anatexis, and tectonic denudation: Geology, v. 18

Webb, A. A. G., Yin, A., Harrison, T. M., Célérier, J., and Burgess, W. P., 2007, The leading edge of the Greater Himalayan Crystalline complex revealed in the NW Indian Himalaya: Implications for the evolution of the Himalayan orogen: Geology, v. 35, no. 10

Yin, A., 2006, Cenozoic tectonic evolution of the Himalayan orogen as constrained by along strike variation of structural geometry, exhumation history, and foreland sedimentation: Earth-Science Reviews, v. 76

Appendix

Garnet Analysis

Label	Ox%(Mg)	Ox%(Al)	Ox%(Si)	Ox%(Ca)	Ox%(Mn)	Ox%(Fe)
1092 gar1-1	2.93	20.68	36.87	10.12	10.60	19.11
1092 gar1-2	3.25	20.70	37.59	10.19	9.56	19.42
1092 gar1-4	3.11	20.66	37.64	10.24	9.93	19.19
1092 gar1-5	2.65	20.60	36.04	9.58	12.97	18.58
1092 gar1-6	2.69	20.63	37.15	9.50	11.88	18.81
1092 gar1 prof-2	2.73	20.63	37.03	9.99	12.17	18.67
1092 gar1 prof-3	2.62	20.89	36.67	9.82	12.43	18.44
1092 gar1 prof-4	2.71	20.77	37.17	9.50	12.52	18.69
1092 gar1 prof-5	2.76	20.66	36.37	8.54	12.71	18.33
1092 gar1 prof-6	2.69	20.81	36.91	9.33	12.39	18.36
1092 gar1 prof-7	2.83	20.63	37.21	8.31	12.23	17.84
1092 gar1 prof-8	2.80	20.63	36.85	9.92	11.69	18.27
1092 gar1 prof-9	2.77	20.68	37.42	10.24	10.78	17.90
1092 gar1 prof-10	2.91	20.45	37.17	10.15	9.59	19.05
1092 gar1 prof2-1	2.78	19.95	37.22	9.62	11.88	18.93
1092 gar1 prof2-2	2.79	20.66	37.23	8.88	12.74	18.65
1092 gar1 prof2-3	2.83	20.89	37.62	8.64	12.77	18.97
1092 gar1 prof2-4	2.69	20.57	37.12	9.76	11.96	18.54
1092 gar1 prof2-5	2.63	20.62	37.34	10.01	12.13	18.27
1092 gar1 prof2-6	2.68	20.76	37.14	10.46	11.15	18.33
1092 gar1 prof2-7	2.88	20.60	37.92	10.59	10.56	18.53
1092 gar1 prof2-8	3.09	20.69	37.11	9.82	10.03	19.46
1092 gar1 prof2-9	3.07	20.75	36.66	9.89	9.82	19.75
1092 gar2r-1	3.13	20.98	36.64	10.14	9.91	19.27
1092 gar2r-2	3.02	20.69	37.03	9.93	10.65	19.13
1092 gar2r-3	3.24	20.82	36.55	9.87	9.78	19.82
1092 gar2c-1	2.60	20.52	37.20	10.44	12.10	18.64
1092 gar2c-2	2.89	20.73	36.36	9.48	11.76	18.83

Label	Ox%(Mg)	Ox%(Al)	Ox%(Si)	Ox%(Ca)	Ox%(Mn)	Ox%(Fe)
1061 gar1r-1	1.43	21.15	36.58	10.92	5.20	24.60
1061 gar1r-2	1.11	20.76	35.54	9.58	9.03	23.62
1061 grt1r-1	1.53	20.79	36.58	11.78	4.78	23.39
1061 grt1r-2	1.44	21.03	37.19	11.84	4.92	23.28
1061 grt1c-1	1.13	20.80	36.94	10.04	8.85	22.73
1061 grt1c-2	1.22	20.90	37.27	10.14	8.26	22.74
1061 grt1p-1	1.46	21.00	36.86	11.20	5.63	23.49
1061 grt1p-2	1.33	21.18	37.46	10.63	6.55	24.30
1061 grt1p-3	1.23	20.94	36.91	10.52	7.04	23.91
1061 grt1p-4	1.20	20.94	37.42	10.24	7.44	23.21
1061 grt1p-5	1.22	20.76	36.64	10.21	7.91	22.82
1061 grt1p-6	1.18	21.10	37.38	10.61	7.91	23.02
1061 grt1p-7	1.09	20.83	36.85	10.34	8.46	22.68
1061 grt1p-8	1.16	20.66	37.31	10.50	8.01	23.01
1061 grt1p-9	1.07	20.99	36.38	10.48	8.10	22.34
1061 grt1p-10	1.19	21.02	36.87	9.99	8.78	22.74
1061 grt1p-11	1.08	20.91	36.44	10.10	8.63	22.66
1061 grt1p-12	1.08	20.88	36.71	9.97	8.76	22.38
1061 grt1p-13	1.11	20.80	36.57	10.14	8.41	22.96
1061 grt1bp-	1.18	20.82	37.31	10.12	8.19	22.80
1061 grt1bp-2	0.99	21.81	37.54	12.75	6.03	20.13
1061 grt1bp-3	1.18	21.02	36.62	10.34	7.15	23.47
1061 grt1bp-4	0.00	11.03	83.42	3.32	0.04	0.33
1061 grt1bp-5	1.25	20.95	36.79	10.64	6.35	23.86
1061 grt1bp-6	1.29	21.17	37.58	11.48	5.72	23.70
1061 grt1bp-7	1.45	20.98	37.15	12.18	4.49	23.62
1061 grt2r-1	1.36	21.20	37.52	11.50	5.63	23.57
1061 grt2r-2	1.38	21.15	37.85	12.11	4.96	23.37
1061 grt2c-1	1.29	21.03	37.08	11.11	5.82	23.25
1061 grt2c-2	1.19	21.09	37.46	10.78	6.38	24.23
972 grt1r-1	0.13	19.72	41.22	12.48	5.41	19.27
972 grt1r-2	0.11	19.88	37.49	14.53	7.18	22.52
972 grt1r-5	0.30	19.17	39.84	10.96	5.83	23.21
972 grt1c-2	0.06	20.81	36.72	16.80	4.28	19.44
972 grt1p-1	0.43	19.16	37.59	12.00	5.67	25.94
972 grt1p-5	0.09	19.66	43.03	12.17	4.82	19.43
972 grt1p-10	0.18	20.04	37.73	14.14	6.57	22.17
972 grt1p-13	0.17	20.04	36.93	13.87	6.50	23.57
972 grt1p-17	0.14	19.97	37.52	14.36	7.05	22.63

Label	Ox%(Mg)	Ox%(Al)	Ox%(Si)	Ox%(Ca)	Ox%(Mn)	Ox%(Fe)
972 grt1p-19	0.12	20.18	40.15	13.51	6.47	20.51
972 grt1p-21	0.30	20.12	36.95	14.05	6.22	23.56
972 grt1p-22	0.21	20.29	37.52	14.21	6.88	22.60
972 grt1p-25	0.20	19.94	36.45	14.18	6.19	22.79
972 grt1p-26	0.35	19.49	37.49	12.24	6.27	25.83
972 grt1p-27	0.14	20.04	36.94	14.68	3.76	24.78
62910 grt1r-2	4.05	20.65	37.39	0.22	0.93	38.61
62910 grt1c-1	4.17	20.75	36.86	0.87	1.75	37.19
62910 grt1c-2	4.04	20.83	36.91	1.16	1.80	36.63
62910 grt1p-1	4.00	20.89	37.28	0.50	1.10	37.99
62910 grt1p-2	4.01	20.78	37.16	1.23	1.15	36.70
62910 grt1p-3	4.01	20.91	37.67	1.01	1.59	36.45
62910 grt1p-4	3.79	20.79	37.08	1.25	1.68	35.96
62910 grt1p-5	3.84	20.73	37.24	1.12	1.91	36.13
62910 grt1p-6	2.48	13.10	59.17	0.71	1.26	24.84
62910 grt1p-7	3.99	20.49	37.33	0.95	1.83	35.55
62910 grt1p-8	3.85	20.40	36.89	0.82	1.82	35.78
62910 grt1p-9	3.94	20.59	37.36	0.84	1.85	35.57
62910 grt1p-10	4.00	20.59	37.30	0.83	1.84	35.96
62910 grt1p-12	3.91	20.88	37.37	1.05	1.77	36.01
62910 grt1p-13	3.81	20.49	37.69	1.26	1.74	35.79
62910 grt1p-14	3.79	20.75	37.22	1.54	1.50	35.71
62910 grt1p-16	4.05	20.50	37.23	0.41	1.01	36.88
62910 grt1p-17	4.06	20.24	37.62	0.24	0.88	36.92

Feldspar Analysis

Label	Ox%(Na)	Ox%(Al)	Ox%(Si)	Ox%(K)	Ox%(Ca)	Ox%(Fe)
1092 kfeld inc-1	4.46	27.29	59.02	0.08	8.27	0.08
1092 kfeld inc-2	5.72	24.65	62.33	0.06	5.45	0.11
1092 kfeld inc-7	5.90	23.98	63.93	0.00	4.29	0.00
1092 kfeld inc t2-2	4.08	27.27	58.69	0.13	8.35	0.04
1092 kfeld inc t2-3	4.28	27.34	58.98	0.15	8.62	0.03
1092 kfeld inc t2-4	4.06	26.86	59.01	0.55	7.59	0.22
1092 kfeld inc t3-1	9.68	24.10	63.61	0.09	4.18	0.01
1092 kfeld inc t3-2	9.47	24.27	63.57	0.11	4.51	0.01
1092 kfeld inc t3-3	10.00	23.56	64.12	0.11	3.41	0.07
1092 kfeld inc t3-5	9.09	24.22	63.49	0.07	4.48	0.00
1061 kfel-1	8.62	24.48	61.57	0.42	5.07	0.02
1061 kfeld1-2	6.34	25.98	61.49	0.17	4.87	0.02
1061 kfeld1-3	8.30	25.75	61.66	0.20	6.07	0.02

Mica Analysis

Analysis	F	Na2O	MgO	Al2O3	SiO2	K2O	CaO	Cl	TiO2
972_bio1	0.26	0.07	7.45	15.40	34.41	8.88	0.03	0.10	2.90
972_bio1	0.35	0.08	7.23	15.11	34.17	9.32	0.05	0.07	3.02
972_bio2	0.43	0.08	7.91	15.35	35.56	9.81	0.00	0.06	3.44
972_bio2	0.37	0.11	8.36	15.65	35.92	9.78	0.00	0.05	3.21
1061_bio1	0.37	0.11	10.82	16.90	36.02	9.50	0.00	0.03	2.20
1061_bio1	0.32	0.07	9.76	16.75	35.69	9.62	0.04	0.02	2.79
1061_bio2	0.44	0.09	11.46	16.68	36.26	9.58	0.03	0.01	1.60
1061_bio3	0.38	0.14	10.69	16.71	36.14	9.62	0.01	0.02	1.89
1061_bio4	0.26	0.05	8.70	16.37	34.83	9.60	0.07	0.02	1.64
1061_bio5	0.40	0.11	10.91	15.86	35.93	9.49	0.00	0.02	1.97
62910_bio1	0.27	0.16	11.28	19.89	36.13	8.96	0.00	0.02	1.32
62910_bio1	0.33	0.18	10.86	20.02	36.02	9.10	0.00	0.02	1.25
62910_musc1	0.07	1.10	0.82	35.74	45.90	9.62	0.00	0.03	0.68
62910_musc1	0.04	1.12	0.89	35.59	46.42	9.66	0.00	0.01	0.62
62910_bio2	0.32	0.08	9.21	19.17	35.43	8.86	0.00	0.02	1.48
62910_bio2	0.32	0.16	9.34	19.04	35.04	9.03	0.00	0.02	1.56
62910_musc2	0.03	1.20	0.75	36.56	46.19	9.67	0.00	0.00	0.50
62910_musc2	0.08	1.20	0.76	36.38	46.27	9.70	0.00	0.00	0.49
62910_bio3	0.30	0.22	10.70	19.47	36.33	8.91	0.01	0.01	1.71
62910_bio3	0.32	0.27	10.90	19.19	35.75	8.70	0.00	0.03	1.76
62910_musc3	0.08	1.17	0.92	35.86	46.71	9.68	0.02	0.00	0.71
62910_musc3	0.09	1.06	1.01	35.33	46.65	9.63	0.04	0.01	0.69

Cont. Mica Analysis

Analysis	FeO	MnO	Cr2O3
972_bio1	25.92	0.33	0.00
972_bio1	25.58	0.35	0.01
972_bio2	23.20	0.34	0.05
972_bio2	22.26	0.34	0.06
1061_bio1	19.58	0.20	0.03
1061_bio1	20.23	0.50	0.06
1061_bio2	18.99	0.32	0.05
1061_bio3	20.27	0.35	0.05
1061_bio4	22.82	0.64	0.11
1061_bio5	20.70	0.32	0.02
62910_bio1	17.42	0.01	0.02

Analysis	FeO	MnO	Cr2O3
62910_bio1	17.21	0.03	0.03
62910_musc1	1.23	0.00	0.06
62910_musc1	1.14	0.01	0.04
62910_bio2	20.46	0.04	0.00
62910_bio2	20.47	0.05	0.03
62910_musc2	1.05	0.01	0.02
62910_musc2	1.16	0.00	0.04
62910_bio3	18.34	0.04	0.03
62910_bio3	17.93	0.03	0.05
62910_musc3	1.29	0.00	0.02
62910_musc3	1.29	0.00	0.04

Amphibole Analysis

Analysis	F	Na2O	MgO	Al2O3	SiO2	K2O	CaO	Cl	TiO2
1092_amph1	0.09	1.49	10.64	13.44	43.00	0.82	11.50	0.01	1.16
1092_amph1	0.08	1.61	10.65	13.39	42.34	0.79	11.45	0.01	1.15
1092_amph1	0.09	1.62	10.84	13.27	42.54	0.82	11.46	0.01	1.14
1092_amph2	0.10	1.57	10.76	13.60	41.90	0.84	11.48	0.01	0.97
1092_amph3	0.10	1.59	8.90	15.31	40.21	1.03	11.45	0.01	0.63
1092_amph3	0.14	1.61	11.00	13.19	42.71	0.79	11.35	0.01	1.07
1092_amph4	0.01	1.59	8.99	15.41	40.03	1.05	11.51	0.02	0.85
1092_amph4	0.13	1.62	10.16	13.98	41.54	0.91	11.50	0.01	1.07
1092_amph5	0.14	1.65	9.36	15.68	40.10	1.02	11.49	0.02	0.71
1092_amph5	0.08	1.63	10.60	13.57	41.73	0.80	11.45	0.01	0.92
972_amph1	0.11	1.40	2.49	13.22	37.41	1.94	10.77	0.14	0.82
972_amph1	0.06	1.30	2.54	12.84	37.77	1.92	11.03	0.18	1.11
972_amph2	0.10	1.44	2.93	13.03	37.98	2.07	10.73	0.18	1.39
972_amph2	0.06	1.48	2.99	13.23	37.70	2.04	10.86	0.17	1.31
972_amph2	0.11	1.65	2.93	13.68	37.85	2.08	10.70	0.19	1.15
972_amph2	0.17	1.55	2.91	13.77	37.65	2.07	10.84	0.16	1.10
972_amph2	0.09	1.50	2.94	13.74	37.85	2.09	10.82	0.20	1.27
972_amph2	0.11	1.61	2.93	13.52	37.82	2.04	10.84	0.20	1.07
972_amph2	0.12	1.52	2.91	13.63	38.04	2.11	10.75	0.18	1.31
972_amph2	0.07	1.56	2.94	13.60	38.10	2.09	10.81	0.19	1.21
972_amph2	0.07	1.41	3.04	13.17	37.96	1.95	10.82	0.15	1.29
972_amph2	0.10	1.35	2.91	13.19	38.05	1.95	10.93	0.14	1.22
1061_amph1	0.19	1.34	8.34	14.19	41.32	1.31	11.74	0.02	0.67

Analysis	F	Na2O	MgO	Al2O3	SiO2	K2O	CaO	Cl	TiO2
1061_amph1	0.16	1.26	8.47	13.77	41.87	1.67	11.72	0.03	0.97
1061_amph2	0.17	1.29	8.20	14.20	41.05	1.84	11.67	0.02	0.92
1061_amph3	0.18	1.26	8.13	14.13	40.79	1.78	11.67	0.01	0.91

Analysis	FeO	MnO	Cr2O3
1092_amph1	14.85	0.70	0.01
1092_amph1	15.09	0.71	0.01
1092_amph1	15.24	0.66	0.01
1092_amph2	15.64	0.71	0.04
1092_amph3	17.06	0.73	0.05
1092_amph3	15.17	0.67	0.01
1092_amph4	16.93	0.81	0.01
1092_amph4	15.87	0.75	0.04
1092_amph5	16.82	0.75	0.02
1092_amph5	15.38	0.74	0.01
972_amph1	28.32	0.53	0.02
972_amph1	28.03	0.56	0.00
972_amph2	27.26	0.44	0.01
972_amph2	27.03	0.44	0.01
972_amph2	26.94	0.38	0.03
972_amph2	27.03	0.42	0.00
972_amph2	26.73	0.46	0.00
972_amph2	26.83	0.45	0.00
972_amph2	27.23	0.42	0.00
972_amph2	27.36	0.42	0.02
972_amph2	27.63	0.40	0.00
972_amph2	27.47	0.38	0.01
1061_amph1	17.82	0.39	0.01
1061_amph1	17.77	0.33	0.07
1061_amph2	18.01	0.36	0.04
1061_amph3	17.88	0.37	0.02